Knebe, A, Pearce, FR, Thomas, PA, Benson, A, Blaizot, J, Bower, RG, Carretero, J, Castander, FJ, Cattaneo, A, Cora, SA, Croton, DJ, Cui, W, Cunnama, D, De Lucia, G, Devriendt, J, Elahi, PJ, Font, AS, Fontanot, F, Garcia-Bellido, J, Gargiulo, ID, Gonzalez-Perez, V, Helly, J, Henriques, B, Hirschmann, M, Lee, J, Mamon, GA, Monaco, P, Onions, J, Padilla, ND, Power, C, Pujol, A, Skibba, RA, Somerville, RS, Srisawat, C, Vega-Martinez, CA and Yi, SK

nIFTy Cosmology: Comparison of Galaxy Formation Models

Article

Mon. Not. R. Astron. Soc. **000**, 1–34 (2010) Printed 19 May 2015 (MN LATEX style file v2.2)

nIFTy Cosmology: Comparison of Galaxy Formation Models

Alexander Knebe,[1⋆] Frazer R. Pearce,[2] Peter A. Thomas,[3] Andrew Benson,[4] Jeremy Blaizot,[5,6,7] Richard Bower,[8] Jorge Carretero,[9,10] Francisco J. Castander,[9] Andrea Cattaneo,[11] Sofia A. Cora,[12,13] Darren J. Croton,[14] Weiguang Cui,[15] Daniel Cunnama,[16] Gabriella De Lucia,[17] Julien E. Devriendt,[18] Pascal J. Elahi,[19] Andreea Font,[20] Fabio Fontanot,[17] Juan Garcia-Bellido,[1,21] Ignacio D. Gargiulo,[12,13] Violeta Gonzalez-Perez,[8] John Helly,[8] Bruno Henriques,[22] Michaela Hirschmann,[23] Jaehyun Lee,[24] Gary A. Mamon,[23] Pierluigi Monaco,[25,17] Julian Onions,[2] Nelson D. Padilla,[28,29] Chris Power,[15] Arnau Pujol,[9] Ramin A. Skibba,[26] Rachel S. Somerville,[27] Chaichalit Srisawat,[3] Cristian A. Vega-Martínez,[12] Sukyoung K. Yi[24]

[1]*Departamento de Física Teórica, Módulo 15, Facultad de Ciencias, Universidad Autónoma de Madrid, 28049 Madrid, Spain*
[2]*School of Physics & Astronomy, University of Nottingham, Nottingham NG7 2RD, UK*
[3]*Department of Physics & Astronomy, University of Sussex, Brighton, BN1 9QH, UK*
[4]*Carnegie Observatories, 813 Santa Barbara Street, Pasadena, CA 91101, USA*
[5]*Universitè de Lyon, Lyon, F-69003, France*
[6]*Universitè Lyon 1, Observatoire de Lyon, 9 avenue Charles Andrè, Saint-Genis Laval, F-69230, France*
[7]*CNRS, UMR 5574, Centre de Recherche Astrophysique de Lyon ; Ecole Normale Supèrieure de Lyon, Lyon, F-69007, France*
[8]*Institute for Computational Cosmology, Department of Physics, University of Durham, South Road, Durham, DH1 3LE, UK*
[9]*Institut de Ciències de l'Espai, IEEC-CSIC, Campus UAB, 08193 Bellaterra, Barcelona, Spain*
[10]*Port d'Informació Científica (PIC) Edifici D, Universitat Autònoma de Barcelona (UAB), E-08193 Bellaterra (Barcelona), Spain.*
[11]*GEPI, Observatoire de Paris, CNRS, 61, Avenue de l'Observatoire 75014, Paris France*
[12]*Instituto de Astrofísica de La Plata (CCT La Plata, CONICET, UNLP), Paseo del Bosque s/n, B1900FWA, La Plata, Argentina.*
[13]*Facultad de Ciencias Astronómicas y Geofísicas, Universidad Nacional de La Plata, Paseo del Bosque s/n, B1900FWA, La Plata, Argentina*
[14]*Centre for Astrophysics and Supercomputing, Swinburne University of Technology, Hawthorn, Victoria 3122, Australia*
[15]*International Centre for Radio Astronomy Research, University of Western Australia, 35 Stirling Highway, Crawley, Western Australia 6009, Australia*
[16]*Physics Department, University of Western Cape, Bellville, Cape Town 7535, South Africa*
[17]*INAF - Astronomical Observatory of Trieste, via Tiepolo 11, I-34143 Trieste, Italy*
[18]*Astrophysics, University of Oxford, Denys Wilkinson Building, Keble Road, Oxford, OX1 3RH, UK*
[19]*Sydney Institute for Astronomy, A28, School of Physics, The University of Sydney, NSW 2006, Australia*
[20]*Astrophysics Research Institute, Liverpool John Moores University, IC2, Liverpool Science Park, 146 Brownlow Hill, Liverpool L3 5RF, UK*
[21]*Instituto de Física Teórica, Universidad Autónoma de Madrid (IFT-UAM/CSIC), 28049 Madrid, Spain*
[22]*Max-Planck-Institut für Astrophysik, Karl-Schwarzschild-Str. 1, 85741 Garching b. München, Germany*
[23]*Institut d'Astrophysique de Paris (UMR 7095: CNRS & UPMC), 98 bis Bd Arago, F-75014 Paris, France*
[24]*Department of Astronomy and Yonsei University Observatory, Yonsei University, Seoul 120-749, Republic of Korea*
[25]*Dipartimento di Fisica, Università di Trieste, via Tiepolo 11, 34143 Trieste, Italy*
[26]*Department of Physics, Center for Astrophysics and Space Sciences, University of California, 9500 Gilman Drive, San Diego, CA 92093*
[27]*Department of Physics and Astronomy, Rutgers University, 136 Frelinghuysen Road, Piscataway, NJ 08854, USA*
[28]*Instituto de Astrofisica, Universidad Catolica de Chile, Santiago, Chile*
[29]*Centro de Astro-Ingenieria, Universidad Catolica de Chile, Santiago, Chile*

Accepted XXXX . Received XXXX; in original form XXXX

ABSTRACT

We present a comparison of 14 galaxy formation models: 12 different semi-analytical models and 2 halo-occupation distribution models for galaxy formation based upon the same cosmological simulation and merger tree information derived from it.

The participating codes have proven to be very successful in their own right but they have all been calibrated independently using various observational data sets, stellar models, and merger trees. In this paper we apply them without recalibration and this leads to a wide variety of predictions for the stellar mass function, specific star formation rates, stellar-to-halo mass ratios, and the abundance of orphan galaxies. The scatter is much larger than seen in previous comparison studies primarily because the codes have been used outside of their native environment within which they are well tested and calibrated.

The purpose of the 'nIFTy comparison of galaxy formation models' is to bring together as many different galaxy formation modellers as possible and to investigate a common approach to model calibration. This paper provides a unified description for all participating models and presents the initial, uncalibrated comparison as a baseline for our future studies where we will develop a common calibration framework and address the extent to which that reduces the scatter in the model predictions seen here.

Key words: methods: N-body simulations – galaxies: haloes – galaxies: evolution – cosmology: theory – dark matter

1 INTRODUCTION

Understanding the formation and evolution of galaxies within a self-consistent cosmological context is one of the outstanding and most challenging topics of astrophysics and cosmology. Over the last few decades great strides forward have been made along two distinct lines: on the one hand, through directly accounting for the baryonic component (gas, stars, supermassive black holes, etc.) in cosmological simulations that include hydrodynamics and gravity and on the other hand, through a procedure known as semi-analytic modelling (SAM), in which a statistical estimate of the distribution of dark matter haloes and their merger history – either coming from cosmological simulations or extended Press-Schechter/Lagrangian methods – is combined with simplified yet physically motivated prescriptions to estimate the distribution of the physical properties of galaxies. To date the vast computational challenge related to simulating the baryonic component has made it impractical for a general adoption of the former approach within the large volumes necessary for galaxy surveys and hence a lot of effort has been devoted to the latter SAM strategy. Further, most of the modelling of sub-grid physics in hydrodynamical simulations relies on schemes akin to the ones used in the SAM approach, and hence it is more effective to apply them in post-processing to a simulation where parameter scans are then less costly. Further, over this period we have not only witnessed significant advances in simulation techniques (e.g. Vogelsberger et al. 2014; Schaye et al. 2015), but the original ideas for SAMs (cf. White & Rees 1978) have undergone substantial refinement too (e.g. Cole 1991; White & Frenk 1991; Lacey & Silk 1991; Blanchard et al. 1992; Kauffmann et al. 1993, and in particular all the people and methods detailed below in Section 3).

Some SAMs simply rely on analytical forms for the underlying merger trees based upon (conditional) mass functions from Press & Schechter (1974) or Extended Press-Schechter (Bond et al. 1991) as, for instance, described in Somerville & Kolatt (1999). Other codes take as input halo merger trees derived from cosmological N-body simulations (see Lacey & Cole 1993; Roukema et al. 1997, for the historical origin of both techniques). While the former remain a critical and powerful approach, advances in computing power (especially for dark matter only simulations) have shifted the focus of SAM developers towards the utilization of N-body merger trees as input to their models as they more reliably capture non-linear structure formation. For a recent comparison of merger tree construction methods, the influence of the underlying halo finder and the impact for (a particular) SAM we refer the reader to results coming out of a previous comparison project 'Sussing Merger Trees'[1] (Srisawat et al. 2013; Avila et al. 2014; Lee et al. 2014): Lee et al. (2014), for instance, have shown that SAM parameters can be re-tuned to overcome differences between different merger trees; something of great relevance for the work presented here, as we will see later.

As well as considering the influence of the halo finder and merger tree construction on any galaxy formation model, it is also important to consider the different semi-analytical techniques and methods themselves. Where this strategy has been used it has thus far focused primarily on comparing the physical details of the model. For instance, Somerville & Primack (1999) (as well as Lu et al. 2011) implemented various physical prescriptions into a single code; by design this tested the underlying physical assumptions and principles rather than for any code-to-code (dis-)similarities. Fontanot et al. (2009) and Kimm et al. (2009) compared different SAMs, but without using the same merger trees as an input. Similarly, Contreras et al. (2013) compared Durham and Munich SAMs for the Millennium simulation (Springel et al. 2005) measuring and comparing the halo occupation distribution found within them. Different channels for bulge formation in two distinct SAMs have been compared by De Lucia et al. (2011) and Fontanot et al. (2011). Fontanot et al. (2012) compared the predictions of three

⋆ E-mail: alexander.knebe@uam.es

[1] http://popia.ft.uam.es/SussingMergerTrees

different SAMs (the same ones as used already in Fontanot et al. 2009; Kimm et al. 2009) for the star formation rate function to observations.

The first move towards using identical inputs was undertaken by Macciò et al. (2010) where three SAMs were compared, this time using the same merger tree for all of them. However, the emphasis was on studying (four) Milky Way-sized dark matter haloes. Díaz-Giménez & Mamon (2010) have analyzed the properties of compact galaxy groups in mocks obtained using three SAMs applied to the same merger trees derived from the Millennium simulation. They found that the fraction of compact groups that were not dense quartets in real space varied from 24% to 41% depending on the SAM. In Snaith et al. (2011) four SAMs (two Durham and two Munich flavours) all based upon trees extracted from the Millennium simulation have been compared with a special focus on the luminosity function of galaxy groups – highlighting differences amongst models, especially for the magnitude gap distribution between first- and second-ranked group galaxies. Stripped down versions of three models (again utilising identical merger trees) have been investigated in great detail by De Lucia et al. (2010): they studied primarily various assumptions for gas cooling and galaxy mergers and found that different assumptions in the modelling of galaxy mergers can result in significant differences in the timings of mergers, with important consequences for the formation and evolution of massive galaxies. Most recently Lu et al. (2014) used merger trees extracted from the Bolshoi simulation (Klypin et al. 2011) as input to three SAMs. They conclude that in spite of the significantly different parameterizations for star formation and feedback processes, the three models yield qualitatively similar predictions for the assembly histories of galaxy stellar mass and star formation over cosmic time. Note that all three models in this study were tuned and calibrated to the same observational data set, i.e. the stellar mass function of local galaxies. Additionally, it should not go unmentioned that a lot of effort has gone into comparing SAMs to the results of cosmological hydrodynamic simulations, either using the same merger trees for both (Yoshida et al. 2002; Helly et al. 2003; Cattaneo et al. 2007; Saro et al. 2010; Hirschmann et al. 2012; Monaco et al. 2014) or not (Benson et al. 2001; Lu et al. 2011) – yielding galaxy populations with similar statistical properties with discrepancies primarily arising for cooling rates, gas consumption, and star formation efficiencies. For an elaborate review of semi-analytical models in relation to hydrodynamic simulations please refer to Somerville & Davé (2014).

In addition to the maturation of SAMs over the past ten years, the field of halo models of galaxy clustering has produced other powerful techniques for associating dark matter haloes with galaxies: the halo occupation distribution (HOD; Jing et al. 1998; Cooray & Sheth 2002), as well as the complementary models of the conditional luminosity function (Yang et al. 2003) and subhalo abundance matching (Conroy et al. 2006). HOD models have been developed to reproduce the observed real-space and redshift-space clustering statistics of galaxies as well as their luminosity, colour, and stellar mass distributions, and they have clarified the similarities and differences between 'central' and 'satellite' galaxies within dark matter haloes. The major difference between SAMs and HODs is that the former model physical processes with merger trees whereas the latter are relating numerical data (for a given redshift) to observations in a statistical manner, i.e. they bypass an explicit modelling of the baryonic physics and rely on a statistical description of the link between dark matter and galaxies. While SAMs are therefore guaranteed to return a galaxy population that evolves self-consistently across cosmic time, HOD models – by construction – provide an accurate reproduction of the galactic content of haloes. In what follows, we refer to both of them as galaxy formation models, unless we want to highlight their differences, and in those cases we again refer to them as SAM or HOD model.

In this work – emerging out of the 'nIFTy cosmology' workshop[2] – we are continuing previous comparison efforts, but substantially extending the set of galaxy formation models: 14 models are participating this time, 12 SAMs and 2 HOD models. We are further taking a slightly different approach: we fix the underlying merger tree and halo catalogue but, for the initial comparison presented here, we allow each and every model to use its favourite parameter set, i.e. we keep the same parameter set as in their reference model based upon their favourite cosmological simulation and merger tree realisation.[3] By doing this we are deliberately not directly testing for different implementations of the same physics, but rather we are attempting to gauge the output scatter across models when given the same cosmological simulation as input. Further, this particular simulation and its trees are different from the ones for which the models were originally developed and tested. By following this strategy, we aim at testing the variations across models outside their native environment and *without* re-tuning. In that regard, it also needs to be mentioned that any galaxy formation model involves a certain level of degeneracy with respect to its parameters (Henriques et al. 2009). This is further complicated by the fact that different models are likely using different parameterizations for the included physical processes. And while it has been shown in some of the previously undertaken comparisons that there is a certain level of consistency (Fontanot et al. 2009; Lu et al. 2014), there nevertheless remains scatter. A study including model re-calibration will form the next stage of this project and will be presented in a future work.

The remainder of the paper is structured as follows: in Section 2 we briefly present the underlying simulation, the halo catalogue and the merger tree; we further summarize five different halo mass definitions typically used. In Section 3 we give a brief description of galaxy formation models in general; a detailed description of each individual model is reserved for Appendix A which also serves as a review of the galaxy formation models featured here. Some general comments on the layout and strategy of the comparison are given in Section 4. The results for the stellar mass function – the key property studied here – are put forward in Section 5 whereas all other properties are compared in Section 6. We present a discussion of the results in Section 7 and close with our conclusions in Section 8.

2 THE PROVIDED DATA

The halo catalogues used for this paper are extracted from 62 snapshots of a cosmological dark-matter-only simulation undertaken using the GADGET-3 N-body code (Springel 2005) with initial conditions drawn from the WMAP7 cosmology (Komatsu et al. 2011, $\Omega_{\rm m} = 0.272$, $\Omega_\Lambda = 0.728$, $\Omega_{\rm b} = 0.0455$, $\sigma_8 = 0.807$, $h = 0.7$, $n_s = 0.96$). We use 270^3 particles in a box of comoving width $62.5h^{-1}\,{\rm Mpc}$, with a dark-matter particle mass of $9.31 \times 10^8 h^{-1}{\rm M}_\odot$. Haloes were identified with SUBFIND (Springel et al. 2001a) applying a Friends-Of-Friends (FOF) linking length of $b = 0.2$ for the host haloes. Only (sub-)haloes with at

[2] http://popia.ft.uam.es/nIFTyCosmology

[3] Note that not all models entering this comparison were designed ab initio to work with N-body trees.

least 20 particles were kept. The merger trees were generated with the MERGERTREE code that forms part of the publicly available AHF package (Knollmann & Knebe 2009; Gill et al. 2004). For a study of the interplay between halo finder and merger tree we refer the interested reader to Avila et al. (2014).

As we run the 14 galaxy formation models with their standard calibration, we have to consider five different mass definitions and provide them in the halo catalogues; three of them are based upon a spherical-overdensity assumption (Press & Schechter 1974)

$$M_{\rm ref}(< R_{\rm ref}) = \Delta_{\rm ref}\rho_{\rm ref}\frac{4\pi}{3}R_{\rm ref}^3 \ , \qquad (1)$$

and two more on the FOF algorithm (Davis et al. 1985). The masses supplied are summarized as follows:

- $M_{\rm fof}$: the mass of all particles inside the FOF group
- $M_{\rm bnd}$: the bound mass of the FOF group
- $M_{\rm 200c}$: $\Delta_{\rm ref} = 200, \quad \rho_{\rm ref} = \rho_{\rm c}$
- $M_{\rm 200m}$: $\Delta_{\rm ref} = 200, \quad \rho_{\rm ref} = \rho_{\rm b}$
- $M_{\rm BN98}$: $\Delta_{\rm ref} = \Delta_{\rm BN98}, \quad \rho_{\rm ref} = \rho_{\rm c}$

where $\rho_{\rm c}$ and $\rho_{\rm b}$ are the critical and background density of the Universe, respectively, both of which are functions of redshift and cosmology. $\Delta_{\rm BN98}$ is the virial factor as given by Eq.(6) in Bryan & Norman (1998), and $R_{\rm ref}$ is the corresponding halo radius for which the interior mean density matches the desired value on the right-hand side of Eq. (1).

Note that SUBFIND returns exclusive masses, i.e. the mass of host haloes does not include the mass of its subhaloes. Further, the aforementioned five mass definitions only apply to host haloes; for subhaloes SUBFIND always returns the mass of particles bound to it.

3 THE GALAXY FORMATION MODELS

The galaxy formation models used in this paper follow one of two approaches, which are either 'semi-analytic model' (SAM) or 'halo occupation distribution' (HOD) based models. We give a brief outline of both below. A far more detailed description of the semi-analytic galaxy formation method can be found in Baugh (2006), whereas Cooray & Sheth (2002) provides a review of the formalism and applications of the halo-based description of non-linear gravitational clustering forming the basis of HOD models.

Both model techniques require a dark matter halo catalogue, derived from an N-body simulation as described above or produced analytically, and take the resultant halo properties as input. Furthermore, SAMs require that the haloes be grouped into merger trees of common ancestry across cosmic time. For SAMs, the merger trees describing halo evolution directly affect the evolution of galaxies that occupy them. HOD models in their standard incarnation do not make use of the information of the temporal evolution of haloes; HOD models rather provides a mapping between haloes and galaxies at a given redshift. However, the utilization of merger trees is in principle possible and there are recent advances in that direction (Yang et al. 2012; Behroozi et al. 2013).

The models and their respective reference are summarized in Table 1 where we also list their favourite choice for the mass definition applied for all the results presented in the main body of the paper. Some of the models also applied one (or more) of the alternative mass definitions and results for the influence on the results are presented in Appendix B. The table also includes information on whether the models included stellar masses and/or a luminosity function during the calibration process. Note that the calibration is not necessarily limited to either or both of these galaxy properties. And we also chose to provide the assumed initial mass function (IMF) in that table which has influences on the stellar masses (and star formation rates) presented later in the paper. However, for more details about the models please refer to Appendix A.

3.1 Semi-analytic galaxy formation models

Semi-analytic models encapsulate the main physical processes governing galaxy formation and evolution in a set of coupled parameterised differential equations. In these equations, the parameters are not arbitrary but set the efficiency of the various physical processes being modelled. Given that these processes are often ill-understood in detail, the parameters play a dual role of both balancing efficiencies and accommodating the (sometimes significant) uncertainties. Their exact values should never be taken too literally. However, a sensible model is usually one whose parameters are set at an order-of-magnitude level of reasonableness for the physics being represented. All models are calibrated against a key set of observables, however exactly which observables are used changes from model to model.

In practice, the semi-analytic coupled equations are what describe how baryons move between different reservoirs of mass. These baryons are treated analytically in the halo merger trees and followed through time. The primary reservoirs of baryonic mass used in all models in this paper include the hot halo gas, cold disk gas, stars, supermassive black holes, and gas ejected from the halo. Additionally, different models may more finely delineate these mass components of the halo/galaxy system (e.g. breaking cold gas into HI and H_2) or even add new ones (e.g. the intra-cluster stars).

The physics that a semi-analytic model will try to capture can typically be broken into the processes below:

- *Pristine gas infall:* As a halo grows its bound mass increases. Most SAMs assume that new dark matter also brings with it the cosmic baryon fraction of new baryonic mass in the form of pristine gas. This gas may undergo heating as it falls onto the halo to form a hot halo, or it may sink to the centre along (cold) streams to feed the galaxy. At early times, infall may be substantially reduced by photoionization heating.
- *Hot halo gas cooling:* A hot halo of gas around a galaxy will lose energy and the densest gas at the centre will cool and coalesce onto the central galaxy in less than a Hubble time. It is usually assumed that this cooling gas conserves angular momentum, which leads to the formation of a cold galactic disk of gas, within which stars can form.
- *Star formation in the cold gas disk:* If the surface density of cold gas in the disk is high enough, molecular clouds will collapse and star forming regions will occur. The observed correlation between star formation rate density and cold gas density or density divided by disk dynamical time can be applied to estimate a star formation rate (Kennicutt 1998).
- *Supernova feedback and the production of metals:* Very massive new stars have short lifetimes and will become supernova on very short timescales. The assumed initial mass function (IMF) of the stars will determine the rate of these events, which will return mass and energy back into the disk, or even blow gas entirely out into the halo and beyond (Dekel & Silk 1986). Supernovae are also

Table 1. Participating galaxy formation models. Alongside the name (first column) and the major reference (last column) we list the applied halo mass definition (second column) and highlight whether the calibration of the model included the stellar mass function (SMF) and/or a luminosity function (LF). Note that the respective model calibration is not necessarily limited to either of these two quantities. We additionally list the assumed initial mass function (IMF). For more details please refer to the individual model descriptions in the Appendix A.

code name	mass	calibration		IMF	reference
GALACTICUS	$M_{\rm BN98}$	SMF	LF	Chabrier	Benson (2012)
GALICS-2.0	$M_{\rm bnd}$	SMF	—	Kennicutt	Cattaneo et al. (in prep.)
MORGANA	$M_{\rm fof}$	SMF	—	Chabrier	Monaco et al. (2007)
SAG	$M_{\rm bnd}$	—	LF	Salpeter	Gargiulo et al. (2014)
SANTACRUZ	$M_{\rm BN98}$	SMF	—	Chabrier	Somerville et al. (2008)
YSAM	$M_{\rm 200c}$	SMF	—	Chabrier	Lee & Yi (2013)
Durham flavours:					
GALFORM-GP14	$M_{\rm bnd}$	—	LF	Kennicutt	Gonzalez-Perez et al. (2014)
GALFORM-KB06	$M_{\rm bnd}$	—	LF	Kennicutt	Bower et al. (2006)
GALFORM-KF08	$M_{\rm bnd}$	—	LF	Kennicutt	Font et al. (2008)
Munich flavours:					
DLB07	$M_{\rm 200c}$	—	LF	Chabrier	De Lucia & Blaizot (2007a)
LGALAXIES	$M_{\rm 200c}$	SMF	LF	Chabrier	Henriques et al. (2013)
SAGE	$M_{\rm 200c}$	SMF	—	Chabrier	Croton et al. (2006)
HOD models:					
MICE	$M_{\rm fof}$	—	LF	'diet' Salpeter	Carretero et al. (2015)
SKIBBA	$M_{\rm 200c}$	—	LF	Chabrier	Skibba & Sheth (2009)

the primary channel to produce and move metals in and around the galaxy/halo system.

• *Disk instabilities:* Massive disks can buckle under their own weight. Simple analytic arguments to estimate the stability of a disk can be applied to modelled galaxies. Unstable disks will form bars that move mass (stars and/or gas) and angular momentum inward. This redistribution of mass facilitates a change in morphology where stars pile up in the centre, leading to the growth of a bulge or pseudo-bulge (Efstathiou et al. 1982; Mo et al. 1998).

• *Halo mergers:* With time haloes will merge, and thus their occupant galaxies will as well. Modern cosmological simulations readily resolve structures within structures, the so-called subhalo (and hence satellite) population. However, not all models use this information, instead treating the dynamical evolution of substructures analytically. Subhaloes can either be tidally destroyed or eventually merge. It also happens that subhaloes will be lost below the mass resolution limit of the simulation, and different models treat such occurrences differently. It is common to keep tracking the now 'orphan' satellites until they merge with the central galaxy.

• *Galaxy mergers and morphological transformation:* Galaxy mergers are destructive if the mass ratio of the two galaxies is close to unity (major merger). In this case the disks are usually destroyed to form a spheroid, however, new accreted cooling gas can lead to the formation of a new disk of stars around it. Less significant mergers (minor mergers) will simply cause the larger galaxy to consume the smaller one. Note that this is a simplified picture and the detailed implementation in a SAM might be based upon more refined considerations (e.g. Hopkins et al. 2009)

• *Merger and instability induced starbursts:* Mergers and instabilities can also produce significant bursts of star formation on short timescales (Mihos & Hernquist 1994b,a, 1996). These are often modelled separately from the more quiescent mode of star formation ongoing in the disk.

• *Supermassive black holes:* Most modern SAMs model the formation of supermassive black holes at the centres of galaxies. Such black holes typically grow through galaxy merger-induced and/or disk instability-induced cold disk gas accretion and/or by the slow accretion of hot gas out of the halo.

• *Active galactic nuclei:* Accretion of gas onto a supermassive black hole will trigger an active phase. For rapid growth this will produce a so-called 'quasar mode' event, typically occurring from galaxy mergers. For more quiescent growth the 'radio mode' may occur. Feedback resulting from the latter has been used by modellers to shut down the cooling of gas into massive galaxies, effectively ceasing their star formation to produce a 'red and dead' population of ellipticals, as observed. Some models also include outflows driven by the 'quasar mode'.

It is important to note that not all the processes above are parameterised. Often simple analytic theory will provide a reasonable approximation for the behaviour of the baryons in that reservoir and their movement to a different reservoir. In other cases an observed correlation between two properties already predicted by the model can be used to predict a new property. However, sometimes there is little guidance as to how a physical process should be captured. In such cases a power-law or other simple relationship is often applied. In many cases parameterization of SAM recipes is also based upon results from numerical experiments. And as we learn more about galaxies and their evolution such prescriptions are updated and refined, in the hope that the model overall becomes a better representation of the real Universe.

Each model used in this paper is described in more detail in Appendix A. There the reader can find references that provide a complete list of the baryonic reservoirs used and a description of the equations employed to move baryons between them.

3.2 Halo occupation distribution models

Halo models of galaxy clustering offer a powerful alternative to the semi-analytic method to produce large mock galaxy catalogues. Therefore and for comparison to the SAMs, respectively, we include them in our analysis. As described in the introduction, halo models may be of three types: halo occupation distribution (HOD); conditional luminosity function (CLF); subhalo abundance matching (SHAM); or some combination or extension of these. Although these models are not equivalent, they tend to have similar inferences and predictions for most galaxy properties and distributions as a function of halo mass and halocentric distance. The two halo models (i.e. MICE and SKIBBA) in this paper are best described as HOD models - even though they both also incorporate subhalo properties and hence feature a SHAM component.

The primary purpose of halo models is to statistically link the properties of dark matter haloes (at a given redshift) to galaxy properties in a relatively simple way. In contrast with SAMs, physical relations and processes are inferred from halo modeling rather than input in the models. By utilizing statistics of observed galaxies and simulated dark matter haloes, halo modelers describe the abundances and spatial distributions of central and satellite galaxies in haloes as a function of host halo mass, circular velocity, concentration, or other properties, and thus provide a guide for and constraints on the formation and evolution of these galaxies.

Given the halo mass function, halo bias, and halo density profile, HOD models naturally begin with the halo occupation distribution, $P(N|M, c\backslash s, x)$, where M is the host halo mass, $c\backslash s$ refers to central or satellite galaxy status, x refers to some galaxy property such as stellar mass or star formation rate. As in SAMs, most models implicitly or explicitly assume that the central object in a halo is special and is (mostly) more massive than its satellites. The mean central galaxy HOD, $\langle N_{\rm c}|M\rangle$, follows an error function, which assumes a lognormal distribution for the central galaxy luminosity (or stellar mass) function at fixed halo mass. The mean satellite galaxy HOD, $\langle N_{\rm s}|M\rangle$, approximately follows a power-law as a function of $(M/M_1)^{\alpha}$, where the parameter $M_1 \propto M_{\rm min}$ and determines the critical mass above which haloes typically host at least one satellite within the selection limits. CLF models have different parameterizations, but the CLFs (or conditional stellar mass functions) may be integrated to obtain HODs. All HOD parameters may evolve with redshift, though in practice, the stellar mass-halo mass relation, for example, evolves very little especially at the massive end. However, the occupation number of satellites as a function of mass evolves significantly.

HOD models are constructed to reproduce conditional distributions and clustering of galaxies from their halo mass distribution, but modeling choices and choices of which constraints to use result in different models having different predictions for relations between galaxies and haloes. In addition, one must make decisions about how and whether to model halo exclusion (the fact that haloes have a finite size and cannot overlap so much so that one halo's center lies within the radius of another halo), scale-dependent bias, velocity bias, stripping and disruption of satellites, buildup of the intracluster light, etc. One can incorporate subhalo properties and distributions, as has been done here (which makes the MICE and SKIBBA models HOD/SHAM hybrids), to model orphan satellites as well. For bimodal or more complex galaxy properties, such as color, star formation rate, and morphology, there is no unique way to model their distributions: hence models have different predictions for the quenching and structural evolution of central and satellite galaxies. Models that incorporate merger trees may have different predictions for galaxy growth by merging vis-a-vis in situ star formation; however, the two models presented here are applied to each snapshot individually.

3.3 Orphan galaxies

'Orphan' galaxies (Springel et al. 2001a; Gao et al. 2004; Guo et al. 2010; Frenk & White 2012) are galaxies which, for a variety of reasons (such as a mass resolution limit and tidal stripping), no longer retain the dark matter halo they formed within. Some of the processes that create orphans are physical. For instance, when a galaxy and its halo enter a larger host halo tidal forces from the latter will lead to stripping of the galaxy's halo. But there are also numerical issues leading to orphan galaxies: halo finders as applied to the simulation data have intrinsic problems identifying subhaloes close to the centre of the host halo (see, e.g., Knebe et al. 2011; Muldrew et al. 2011; Onions et al. 2012) and therefore the galaxy's halo might disappear from the merger tree (see Srisawat et al. 2013; Avila et al. 2014). As, unless they have merged, galaxies do not simply disappear from one simulation snapshot to the next, the majority of the SAMs deal with this by keeping the galaxy alive and in their catalogues. They evolve associated properties such as position and velocity in different ways: some teams freeze these at the values they had when the host halo was last present while others integrate their orbits analytically or tag a background dark matter particle and follow that instead. Note that information about the motion of dark matter particles was not supplied to the modellers during the comparison and so this latter method was not available in this study. For that reason we do not include any analyses which are affected by the choice of how to assign positions and velocities to orphans.

3.4 Calibration

For the initial comparison presented here we do not require a common calibration, but rather each semi-analytical model is used 'as is'. In particular this means that each model has been run with its preferred physical prescriptions and corresponding set of parameters, as detailed in the Appendix, *without specific retuning*. One of the purposes in doing this is to show the importance of providing adequate calibraton when applying the models. We show in Section 5 that the raw scatter in the stellar mass function is very large but reduces considerably when models use their preferred merger tree/halo mass definition and initial-mass-function. A detailed comparison of models when retuned to match the nIFTy merger trees and halo catalogues will be the topic of a future paper.

4 THE COMPARISON

First we present our methodology and establish the terminology used throughout the remainder of the paper. We illustrate in Fig. 1 how galaxies and the haloes they live within are connected. A circle represents a dark matter halo, a horizontal line a galaxy. A solid arrow points to the host halo of the galaxy whereas a dashed arrow points to the main halo the galaxy orbits within. Note that any substructure hierarchy has been flattened to one single level, i.e. sub-subhaloes will point to the highest level main halo. The sketch also includes orphan galaxies which will have a pointer to its 'last' dark matter host halo.

To facilitate comparison, in all subsequent plots that make use of halo mass we (arbitrarily) chose $M_{\rm bnd}$ regardless of the mass

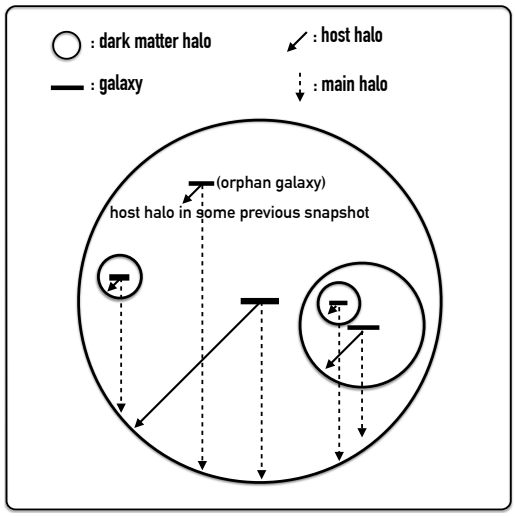

Figure 1. Sketch illustrating the population of galaxies residing inside a dark matter 'main halo' (outermost circle). Each galaxy can have its own dark matter halo which we will refer to as 'host halo' (or simply 'halo'). Galaxies can also be devoid of such a 'galaxy host halo' and then they are tagged as an 'orphan' galaxy.

definition used internally by each model. Each galaxy in the supplied galaxy catalogues points to its host halo (either the present one, if it still exists, or its last one in the case of orphans) and this link is used to select $M_{\rm bnd}$ from the original halo catalogue – irrespective of the mass definition used in the actual model. This allows us to directly compare properties over a single set of halo masses without concern that the underlying dark matter framework has shifted slightly or is evolving differently with redshift.

We have further limited all of the comparisons presented here to galaxies with stellar masses $M_* > 10^9 h^{-1}{\rm M}_\odot$ – a mass threshold appropriate for simulations with a resolution comparable to the Millennium simulation (see Guo et al. 2011). Additionally, when connecting galaxies to their haloes we have applied a mass threshold for the latter of $M_{\rm halo} > 10^{11} h^{-1}{\rm M}_\odot$, corresponding to approximately 100 dark matter particles for the simulation used here.

When interpreting the plots we need to bear in mind – as can be verified in Appendix A – that a great variety of model calibrations exist: some models tune to stellar mass functions (SMF), some models to luminosity functions (LF), and the HOD models to the clustering properties of galaxies. To facilitate the differentiation between calibrations in all subsequent plots we chose colours for the models as follows: models calibrated using only SMFs are presented in blue, models calibrated using LFs in red, and models using a combination of both in green; the 2 HOD models are shown in black, but with different linestyles.

Note that not all models necessarily appear in all plots. For instance, the SKIBBA HOD model only provided a galaxy catalogue for redshift $z = 0$ and hence is not shown in evolutionary plots. Some models do not feature orphans and so do not appear in the corresponding plots.

For the comparison presented in this first paper we now focus on the stellar mass function (SMF) to be presented in the following Section 5. There we will also investigate several origins for model-to-model variations seen not only for the SMF, but also for other galaxy properties to be presented in Section 6, e.g. star formation rates, number density of galaxies, orphan fractions, and the halo occupation. We deliberately exclude luminosity-based properties as

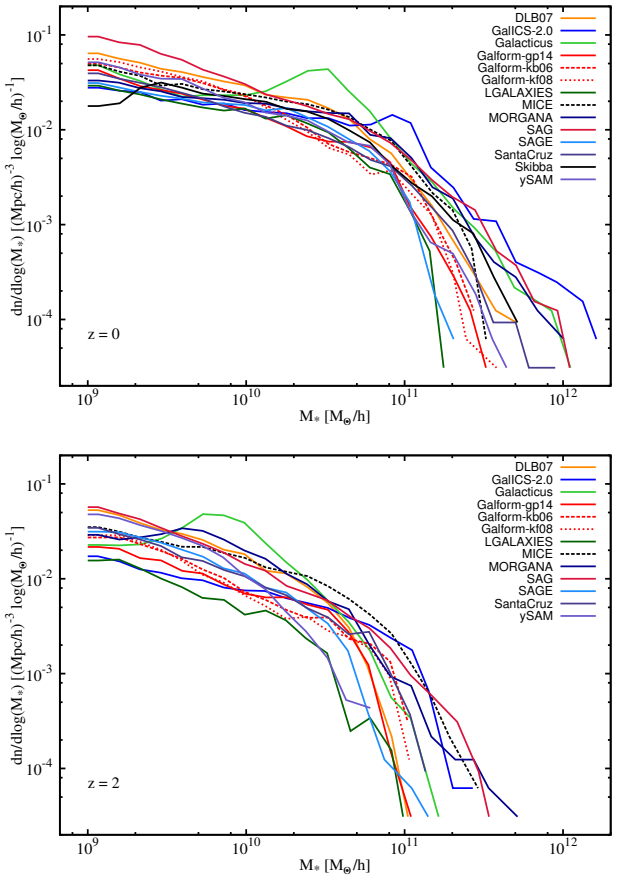

Figure 2. Stellar mass function at redshift $z = 0$ (top) and $z = 2$ (bottom). Each model used its preferred mass definition and initial stellar mass function.

they introduce another layer of modelling, i.e. the employed stellar population synthesis and dust model.

5 STELLAR MASS FUNCTION

A key property, used by many of the models presented here to constrain their parameters, is the stellar mass function of galaxies: we therefore dedicate a full section to its presentation and discussion. It is shown in Fig. 2 both at redshift $z = 0$ (top panel) and $z = 2$ (bottom panel). This plot indicates that there is quite a range in both galaxy abundance and mass (influenced by star formation rate and star formation history) across the models. These differences are apparent at $z = 0$ where the models are calibrated, but are even more pronounced at redshift $z = 2$. At $z = 0$ the model results vary in amplitude by around a factor of 3 in the main and exhibit high mass cut-offs of varying steepness and position; at $z = 2$ the differences in amplitude are even larger, reflecting a broad variation in the location of the peak in star formation rates (presented in the next section).

The HOD model MICE lies within the range of stellar mass functions provided by the SAMs as does the SKIBBA model above $10^{9.5} h^{-1}{\rm M}_\odot$. At $z = 2$ the SKIBBA model does not provide a return while the MICE model features amongst the models with the largest number of high mass galaxies, i.e. the MORGANA and SAG models. While in MORGANA the overproduction of massive

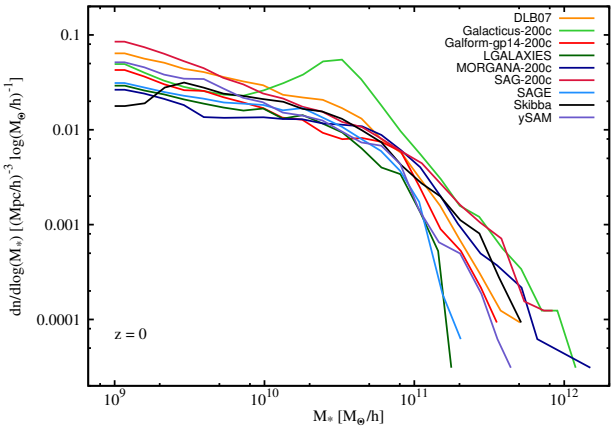

Figure 3. Stellar mass function at redshift $z = 0$ for models that (also) returned galaxy catalogues using M_{200c} as the mass definition. To be compared against the upper panel of Fig. 2

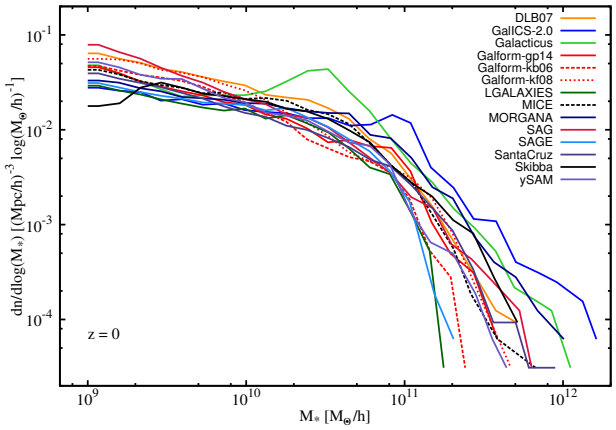

Figure 4. Stellar mass function at redshift $z = 0$ after applying a correction for the applied IMF, i.e. models have been corrected towards a Chabrier IMF. To be compared against the upper panel of Fig. 2

galaxies is connected to the inefficiency of the chosen AGN feedback implementation to quench cooling in massive haloes, in SAG and MICE it could additionally be related to the assumption of a Salpeter IMF which implies a higher mass estimate than for a Chabrier IMF (see Section 5.2 below). The mass function for LGALAXIES at $z = 2$ is lower than any other model due to the delayed reincorporation of gas ejected from supernova feedback that shifts star formation in low mass galaxies to later times (Henriques et al. 2013). At both redshifts the GALACTICUS model displays a bump in the stellar mass function around $10^{10}h^{-1}\mathrm{M}_{\odot}$ due to the matching of feedback from active galactic nuclei and supernovae. For completeness we also checked that the scatter seen here basically remains unchanged when restricting the analysis to (non-)central galaxies and (non-)orphans, respectively.

The differences seen here are huge, especially at the high-mass end, even when models have implemented the same physical phenomena such as supernova and AGN feedback. For instance, LGALAXIES and GALACTICUS both allow the black hole to accrete from the hot halo, with associated jets and bubbles producing 'radio mode' feedback: however, the mass of the largest galaxies differs by around an order of magnitude at redshift $z = 0$. In order to understand how much of this difference arises from the different physical implementations, we first need to consider other factors that may influence the results. For example, the models:

a) use a variety of halo mass definitions;
b) use different initial-mass functions (IMFs);
c) have been taken out of their native environment, i.e. they have been applied to a halo catalogue and tree structure that they were not developed or tested for;
d) have not been re-calibrated to this new setup; and
e) have not been tuned to the same observational data.

In the following sub-sections we will address points a-c) in more detail. Points d) and e) are more complex and will be left for a future study.

5.1 Mass Definition

It can be seen from Table 1 that the models participating in this comparison applied a variety of different mass definitions (which were introduced in Section 2) to define the dark matter haloes that

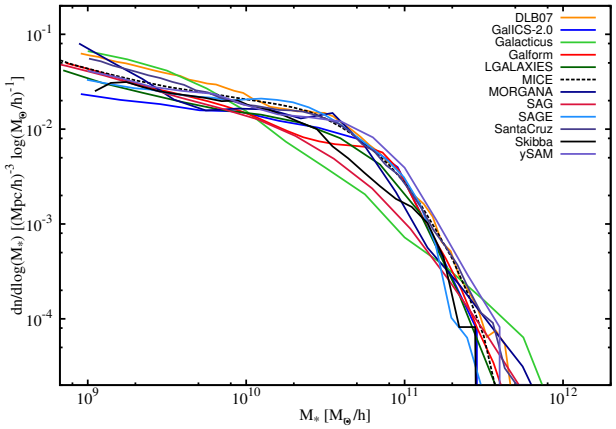

Figure 5. Stellar mass function at redshift $z = 0$ for all the models when created in the native environment used during the model calibration. All curves have been corrected for the IMF towards Chabrier. This figure uses the same scale as (and should be compared to) Fig. 4.

formed their halo merger tree. But as several of the code representatives also returned galaxy catalogues using mass definitions other than their default one, we are able to prepare a plot that shows the stellar mass function for M_{200c}, i.e. the mass definition for which the maximum number of models exist. We show that plot as Fig. 3 where we see that the effect of changing the mass definition is smaller than the model-to-model variation and hence not the primary source of it.

Appendix B provides a direct comparison of models for two different mass definitions (their standard one and M_{200c}). That appendix further shows its influence on other galaxy properties such as the stellar-to-halo mass ratio and the number and star formation density evolutions.

5.2 IMF Correction

An additional source of scatter is that the models assumed various initial stellar mass functions. Hence we transformed the stellar masses returned by each model to a unified Chabrier IMF (Chabrier 2003). For that we used the following equations (Mitchell et al.

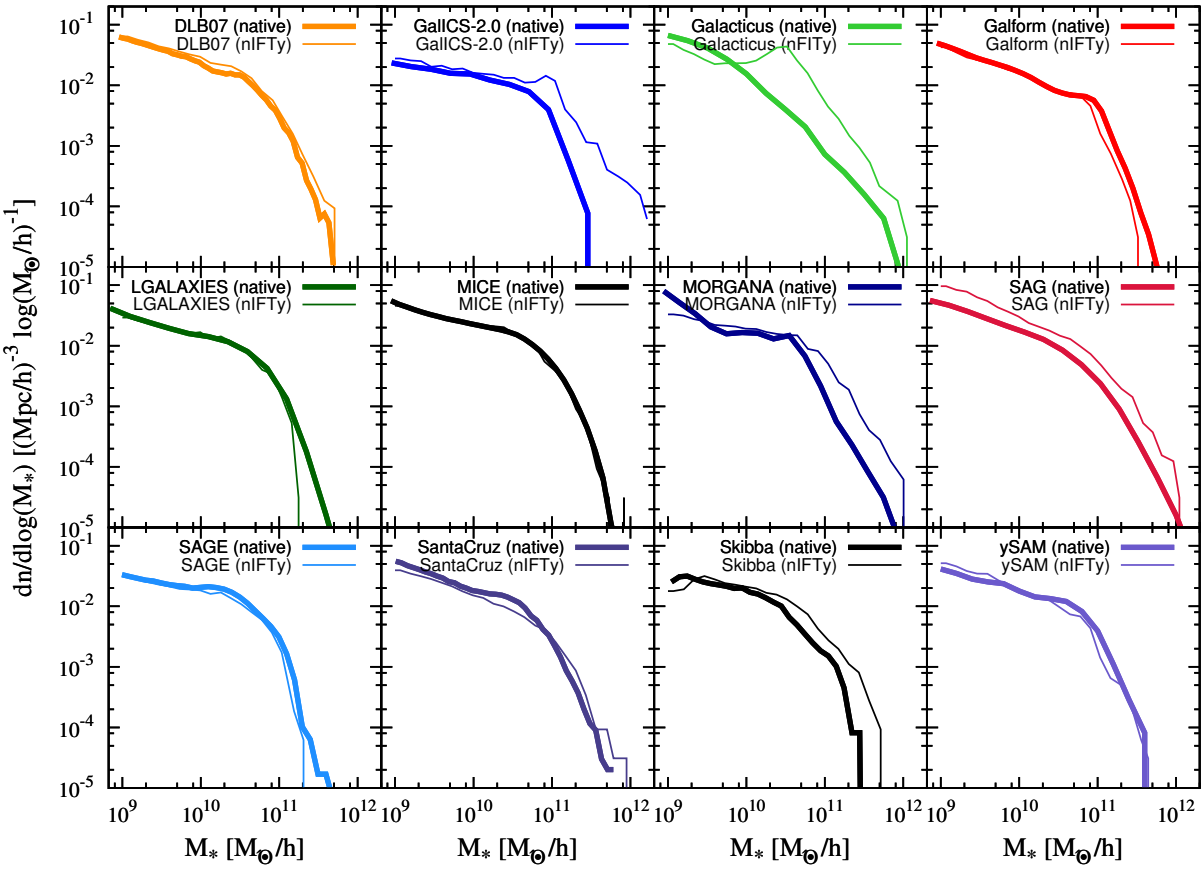

Figure 6. Comparing the stellar mass functions for each model as given in its native environment (thick lines) and when applied with the same parameters to the nIFTy data (thin lines).

2013; Bell & de Jong 2001):

$$\begin{aligned} \log_{10}(M_*^{\rm Chabrier}) &= \log_{10}(M_*^{\rm Salpeter}) - 0.240 \\ \log_{10}(M_*^{\rm Chabrier}) &= \log_{10}(M_*^{\rm diet-Salpeter}) - 0.090 \\ \log_{10}(M_*^{\rm Chabrier}) &= \log_{10}(M_*^{\rm Kennicutt}) + 0.089 \end{aligned} \quad (2)$$

Note that this is only a rough correction, as these numbers depend on the stellar population synthesis (SPS) model, age and metallicity of the simple stellar population and on looking to one or several bands when estimating stellar masses from broad band photometry.

The models have been corrected as follows:

- GALICS-2.0: tuned to observations w/ Chabrier IMF;
- GALFORM: Kennicut → Chabrier;
- MICE: diet-Salpeter → Chabrier;
- SAG: Salpeter → Chabrier;

noting that we left GALICS-2.0 untouched because this model tuned its parameters to an observational data that itself assumed already a Chabrier IMF.

In Fig. 4 we show the resulting stellar mass function for all models where we notice again that the scatter is only slightly reduced. Some additional information is again provided in Appendix C.

5.3 Model Environment

While the whole idea of the comparison presented in this paper is to apply galaxy formation models to the same halo catalogues and merger trees coming from a unique cosmological simulation, we have seen that there is a non-negligible scatter across properties. This scatter is larger than in previous comparison projects which encompassed fewer models (e.g. Kimm et al. 2009; Fontanot et al. 2009, 2012; Contreras et al. 2013; Lu et al. 2014). As we could neither attribute the increased variations to halo mass definitions nor the assumed initial stellar mass functions we are now going to show that this in part comes from taking models out of their native environment. The majority of the models have been designed using a certain simulation and tree structure. However for the comparison presented here this environment has often been substantially changed, and model parameters have not been adjusted to reflect this (as mentioned before, such a recalibration will form part of the follow-up project). The effect of this approach can be appreciated in the two following plots.

Fig. 5 shows the stellar mass functions at redshift $z = 0$ for all models *as given when applied to the simulation and merger trees used for calibration*; we refer to this setup as 'native environment'. These data points were directly provided by the code representatives, then converted to a common IMF, as in the previous section, and plotted on the same axes/scale as for Fig. 2. The agreement between the models is now much improved indicating that the main part of the scatter seen before is due to models being applied to

simulation data they were not adapted to (and that might even feature a different cosmology). There are still a few outliers on the low-mass end, e.g. GALICS-2.0: this model was calibrated on the UltraVISTA SMFs at different redshifts, not on local mass functions; and models calibrated on high-z data tend to underestimate the low-mass end of the local SMF.

To underline the influence of the merger trees to the model results we directly compare in Fig. 6 the native (thick lines) to the nIFTy (thin lines) stellar mass function where each panel represents one model. This plot quantifies the sensitivity of the model to the underlying simulation and merger tree. It shows that *recalibration is required whenever a new simulation is to be used*. While this is common practice within the community, its necessity has been shown here for the first time. A forthcoming companion paper will further address the influence of the applied observational data set to the remaining model-to-model scatter.

6 GALAXIES AND THEIR HALOES

In this section we extend the comparison to several additional properties including star formation rate, the stellar mass fraction, the number density (evolution) of galaxies, and the relation between galaxies and their dark matter haloes.

6.1 Star formation rate

The stellar mass of a galaxy studied in the previous section depends upon the evolution of its star formation rate (SFR). Therefore we now turn to the history of the star formation rate across all considered models. In Fig. 7 we show the redshift evolution, noting that all the curves in this plot have been normalized by their redshift $z = 0$ values (which are given in the third column of Table 2). In this way we separate trends from absolute differences. An unnormalized version of Fig. 7 can be found in Appendix D. Remember that the HOD model SKIBBA does not produce high redshift outputs and so appears neither in Fig. 7 nor in the SFR columns of the accompanying Table 2.

For the SAMs the peak of star formation is about redshift $z \sim 2-3$ followed by a rapid decrease at late times – in agreement with observations and the uncertainties seen within them (e.g. Madau & Dickinson 2014). But amongst these models there are also differences: in LGALAXIES, for instance, the peak is at smaller redshifts while for GALACTICUS it is at earlier times; and the HOD model MICE shows a relatively high SFR at low redshifts, i.e. MICE stars are formed preferentially later than in the other models. These differences are reflected in the fact that, given the redshift $z = 0$ normalisation in the plot, there are differences in amplitude of an order of magnitude at redshift $z > 6$.

While the previous figure has shown the integrated star formation rate, we inspect its redshift $z = 0$ properties more closely in Fig. 8 where we present the star-formation-rate distribution function, i.e. the number density of galaxies in a certain SFR interval. From that we see that all models have a similar functional form, but that the normalisation of the SFR shows differences of up to a factor of three between models. This is reflected in Table 2 where we list the total stellar mass formed (second column), the present-day star formation rate (third column) and specific star formation rate (last column, i.e. the ratio between SFR and total M_*). We see that, for instance, the GALACTICUS model produced more than three times as many stars as LGALAXIES.

The two previous figures showed the overall star formation

Table 2. Total stellar mass, star formation rate, and global specific star formation rate in galaxies with $M_* > 10^9 h^{-1}\mathrm{M}_\odot$ at redshift $z = 0$ (computed as total stellar mass divided by total SFR).

code name	M_* $[10^{14}h^{-1}\mathrm{M}_\odot]$	SFR $[10^4 h^{-1}\mathrm{M}_\odot \mathrm{yr}^{-1}]$	sSFR Gyr^{-1}
GALACTICUS	2.91	2.22	0.0761
GALICS-2.0	2.73	0.88	0.0321
MORGANA	1.96	1.21	0.0614
SAG	2.37	1.15	0.0486
SANTACRUZ	1.11	0.53	0.0475
YSAM	1.14	0.85	0.0749
Durham flavours:			
GALFORM-GP14	0.98	0.50	0.0511
GALFORM-KB06	1.16	0.51	0.0442
GALFORM-KF08	1.06	0.52	0.0491
Munich flavours:			
DLB07	1.76	0.99	0.0563
LGALAXIES	0.87	1.07	0.1234
SAGE	1.01	0.83	0.0815
HOD models:			
MICE	1.77	0.96	0.0543
SKIBBA	1.49	n/a	n/a

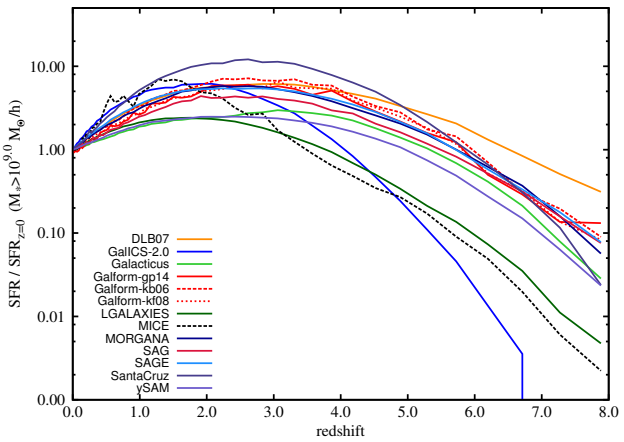

Figure 7. Star formation rate density for galaxies with $M_* > 10^9 h^{-1}\mathrm{M}_\odot$ as a function of redshift (normalized to the redshift $z = 0$ values listed in Table 2).

rate, but now we focus in Fig. 9 on the *specific* star formation rate (sSFR) as a function of stellar mass M_* at redshift $z = 0$. The left panel shows the sSFR excluding passive galaxies, i.e. galaxies that are not considered 'star-forming', which we define as those with sSFR < 0.01 Gyr^{-1}. Points shown are the mean values in the bin, both for the y- and x-axes, (which explains why they do not start exactly at our mass threshold of $10^9 h^{-1}\mathrm{M}_\odot$).[4] Instead of error bars, the right panel of Fig. 9 shows the distribution of sSFR values for a mass bin $M_* \in [10^{10}, 10^{11}] h^{-1}\mathrm{M}_\odot$ with our

[4] Although not shown we also reproduced the plot using medians and 25 and 75 percentiles, but as these give very similar results we decided to adopt mean values for this and all subsequent plots.

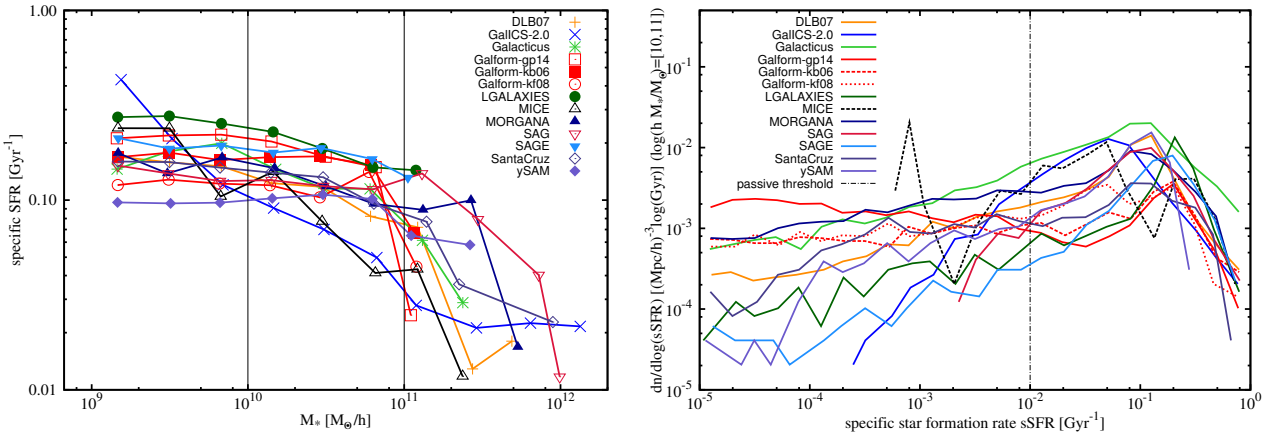

Figure 9. Specific star formation rate of star-forming galaxies at redshift $z = 0$. The left panel shows the star formation rate per stellar mass as a function of stellar mass M_*; points represent mean values binned in both the y and x direction for the star forming sequence of galaxies. The right panel serves as a proxy for the (omitted) error bars: it shows the distribution of specific star formation rates for galaxies in the mass range $M_* \in [10^{10}, 10^{11}]h^{-1}\mathrm{M}_\odot$ (indicated by the two vertical lines); the vertical dashed line indicates our choice for the passive galaxy fraction threshold.

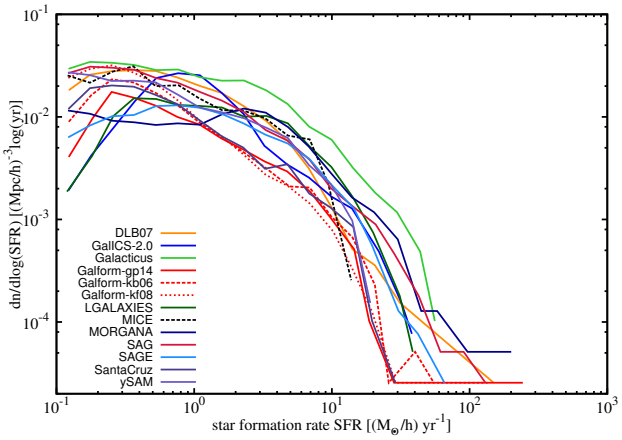

Figure 8. Star formation rate distribution function at redshift $z = 0$.

choice for the passive threshold shown as a vertical dotted line. We are aware that the choice of this mass bin for the right panel encompasses the 'knee' of the stellar mass function, but this right panel nevertheless shows that our passive threshold value cuts the wing to the left at approximately the same height as the right side. Please note that the right panel does not substantially change when considering a different mass range, although this is not explicitly shown here.

Fig. 9 reflects what has already been seen in Fig. 7, i.e. there is a great diversity in star formation rates across the models irrespective of the stellar mass of the galaxy. Bearing in mind the differences in stellar mass functions visible here again on the x-axis, the curves vary by a factor of about 3 at essentially all masses, with the primary difference being in overall normalisation.

We would like to remark on the interplay between Fig. 7, Table 2 and Fig. 9 as at first sight the results seem to be counterintuitive. For instance, GALACTICUS has a much higher star formation rate (at all times) than LGALAXIES, yet the specific star formation rate is higher for LGALAXIES. This is readily explained by the presence of, on average, more massive galaxies in GALACTICUS, which is confirmed by the stellar mass function presented in Fig. 2. One should also bear in mind that the specific star formation rate sSFR could be considered a proxy for the (inverse of the) age of a galaxy. Therefore, Fig. 9 indicates, for example, that it took galaxies in LGALAXIES less time to assemble their stellar mass than galaxies in GALACTICUS.

We close our discussion of Fig. 9 with the remark that it does not change when considering only centrals: the differences across models remain unaffected by restricting the analysis to this galaxy population. However, the specific star formation rate rises, with approximately constant ratios between the curves, when moving to higher redshifts.

6.2 Stellar mass fractions

In Fig. 10 we show the stellar-to-halo mass ratio $M_*/M_{\rm halo}$ as a function of galaxy host halo mass $M_{\rm halo}$ for non-orphan galaxies.[5] The layout of this figure is similar to the previous one, i.e. the left panel shows the actual mean of the ratios (omitting error bars), with the distribution of the values in a galaxy host halo mass bin $M_{\rm halo} \in [10^{12}, 10^{13}]h^{-1}\mathrm{M}_\odot$ the right serving as a proxy for the missing error bars. All models have a similar maximum stellar mass fraction of about 0.1, but there is a large spread in the modal value and this leads to a difference in overall normalisation of approximately a factor of 3 – where some of this variation can be attributed to the different mass definitions applied (see Appendix B). Note that the curves remain unaffected by restricting the data to central galaxies only. Further, the distributions shown in the right panel are not influenced by the halo mass bin.

6.3 Number density

Turning to the galaxies themselves we show in Fig. 11 the evolution of the number density of galaxies (with stellar mass in excess of $M_* > 10^9 h^{-1}\mathrm{M}_\odot$) as a function of redshift – normalized to the number of galaxies at redshift $z = 0$ (provided in Table 3).[6] It is noteworthy that the various models display different evolutionary trends of galaxy density. For instance, DLB07 starts with the

[5] We omit orphan galaxies as they lack an associated halo mass.
[6] Note that as the SKIBBA model solely provides $z = 0$ data it does not appear in the figure.

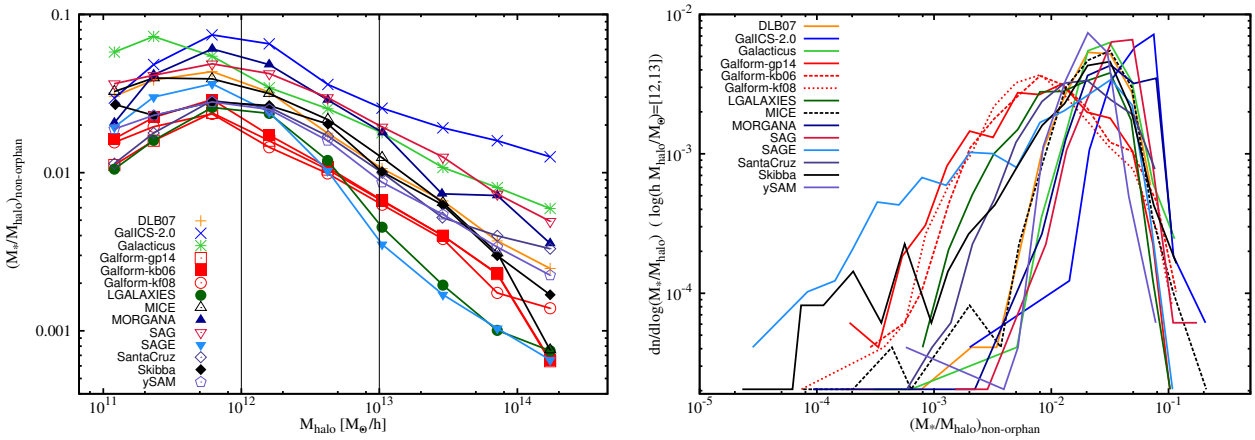

Figure 10. Stellar-to-halo mass ratio for all (non-orphan) galaxies at redshift $z = 0$. The left panel shows mean values (again in both directions) as a function of galaxy host halo mass $M_{\rm halo}$ whereas the right panel indicates the (omitted) error bars: it shows the distribution of $M_*/M_{\rm halo}$ for galaxy halo masses in the range $M_{\rm halo} \in [10^{12}, 10^{13}]h^{-1}{\rm M}_\odot$.

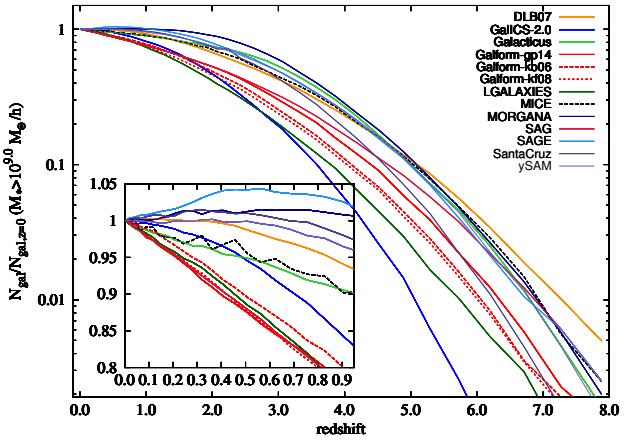

Figure 11. The number of all galaxies with stellar mass $M_* > 10^9 h^{-1}{\rm M}_\odot$ (normalized to redshift $z = 0$ values as listed in Table 3) as a function of redshift. The inset panel shows a zoom (using a linear y-axis) into the range $z \in [0, 1]$.

largest fraction of galaxies at high redshift whereas GALICS-2.0 begins with the lowest fraction – with the difference being more than one order of magnitude at redshift $z = 6$ between these two models. We further note (in the inset panel) that some of the models – in particular SAGE – have a flat or falling galaxy number density between a redshift $z = 1$ and the present day – this is perfectly allowable as galaxy merging can reduce the galaxy density. Although not explicitly shown here, the main features of the plot remain the same when restricting the analysis to central galaxies only.

Fig. 11 should be viewed together with Table 3 as the former provides the trend whereas the latter quantifies the normalization (at redshift $z = 0$); for a combination of both, i.e. an un-normalized version of Fig. 11, we refer the reader to Fig. D2 in the Appendix. The total number of galaxies with $M_* > 10^9 h^{-1}{\rm M}_\odot$ ranges from $\approx$ 7500 for the LGALAXIES model to $\approx$15000 in the DLB07 model. All models (apart from SKIBBA) populate all dark matter (sub-)haloes found in the simulation down to at least $M_{\rm halo} \approx 10^{11} h^{-1}{\rm M}_\odot$. Hence, any differences seen here originate from lower mass objects. This is confirmed by re-calculating $N_{\rm central}$ applying a halo mass threshold of $M_{\rm halo} > 2 \times 10^{11} h^{-1}{\rm M}_\odot$ (instead of the galaxy stellar mass threshold of $M_* > 10^9 h^{-1}{\rm M}_\odot$). This process results in 3774 galaxies for all models – a number identical to the number of host haloes in the SUBFIND catalogue above this mass limit.

Table 3. Number of galaxies at redshift $z = 0$ with a stellar mass in excess of $M_* > 10^9 h^{-1}{\rm M}_\odot$. (For the MORGANA and SANTACRUZ models the number of orphans is in fact the number of satellite galaxies, see text.)

code name	$N_{\rm gal}$	$N_{\rm central}$	$N_{\rm non-orphan}$	$N_{\rm orphan}$
GALACTICUS	14255	7825	10019	4236
GALICS-2.0	9310	7462	9310	0
MORGANA	10008	6186	6186	*3822*
SAG	19516	13571	16256	3260
SANTACRUZ	8901	6682	6682	*2219*
YSAM	11138	7423	9458	1680
Durham flavours:				
GALFORM-GP14	8824	5097	6098	2726
GALFORM-KB06	11563	6669	7897	3666
GALFORM-KF08	12116	6430	7664	4452
Munich flavours:				
DLB07	15132	9420	11897	3235
LGALAXIES	7499	4792	6287	1212
SAGE	8437	6588	8437	0
HOD models:				
MICE	12191	7286	10106	2085
SKIBBA	9203	5088	7973	1230

In Table 3 we further divide the galaxies into different populations, i.e. centrals, non-orphans, and orphans. The fraction of orphan galaxies also shows a spread from a mere 13 per cent for SKIBBA to nearly 37 per cent for the GALFORM-KF08 model. Note that GALICS-2.0, and SAGE do not feature orphans at all, whereas the MORGANA and SANTACRUZ models, as previously mentioned, do not make use of the N-body information for subhaloes and hence tag satellite galaxies as orphans – therefore all satellite galaxies in these models are technically orphans as only central galaxies retain information about their host halo; naturally,

$N_{\rm central} = N_{\rm non-orphan}$ for these two models. To further explore the differences in the abundance of orphan galaxies between models we show in the upper (lower) panel of Fig. 12 the number (stellar mass) fraction of all galaxies that are classified as non-orphans with stellar mass in excess of $M_* > 10^9 h^{-1}{\rm M}_\odot$ orbiting inside a main halo of given mass $M_{\rm halo}$.[7] We can observe some bimodality here: the two HOD models have the lowest fraction of orphans in high-mass main haloes (cf. Table 3) whereas for all other models orphans form the dominant population, making up between 40 and 75 per cent of all galaxies at $z = 0$ within main haloes above $M_{\rm halo} > 10^{13} h^{-1}{\rm M}_\odot$. This trend is also true at higher redshifts although we do not explicitly show it here. For those models which feature orphans, the variation in the number of orphans is due to the various methods of dealing with their eventual fate: over some timescale orphans are expected to suffer from dynamical friction and merge into the central galaxy of the halo. This timescale can be very long in some models (see e.g. De Lucia et al. 2010). The basic features of the plot do not change when applying a more strict threshold for M_* as can be verified in the lower panel of Fig. 12 where we show the stellar mass weighted fraction of non-orphan satellite galaxies. However, now the model variations are reduced. The difference from unity is the fraction of stellar mass locked up in orphans, still as large as 60 per cent for the GALFORM models, yet substantially smaller than the number fraction presented in the top panel. These differences might be ascribed to the different treatment of merger times again. We also observe that for the HOD models the orphan contribution has nearly vanished when weighing it by stellar mass.

6.4 Galaxy-Halo Connection

Lastly, we now turn to how the supplied tree hierarchy has been populated with galaxies by each model. To this extent the upper panel of Fig. 13 compares the supplied halo mass function (crosses, all identified objects down to 100 particles including subhaloes) overplotted by the halo mass function as derived from the galaxy catalogues returned by the models. Note that the MORGANA and SANTACRUZ models have been omitted due to their treatment of subhaloes. While the logarithmic scale of the upper panel masks any differences, the lower panel – showing the fractional difference of each model's halo mass function with respect to the supplied input mass function – indicates that nearly every (sub-)halo found in the simulation contains a galaxy. The only exception to this is the SKIBBA model, which has a high incompleteness threshold that frequently leaves small haloes empty. For the other models differences are all below 2 per cent.

In Fig. 14 we relate the number of galaxies with stellar mass $M_* > 10^9 h^{-1}{\rm M}_\odot$ to the mass of the dark matter main halo they orbit within. We normalize the average number of galaxies by the mass of the main halo, i.e. presenting the 'specific frequency of galaxies'. The solid line running from the upper left to the lower right across the plot indicates a frequency of 'one galaxy per main halo'. Haloes to the right of this line essentially always contain at least one galaxy while the values to the left are indicating the fraction of haloes devoid of galaxies and are chiefly driven by incompleteness – and in retrospect justifying our threshold of $M_{\rm halo} > 10^{11} h^{-1}{\rm M}_\odot$ for the previous plots. At high halo mass, $M_{\rm halo} > 10^{13} h^{-1}{\rm M}_\odot$, the specific frequency of galaxies

[7] As neither GALICS-2.0, MORGANA, SAGE, nor SANTACRUZ feature orphans, they have been omitted from the plot.

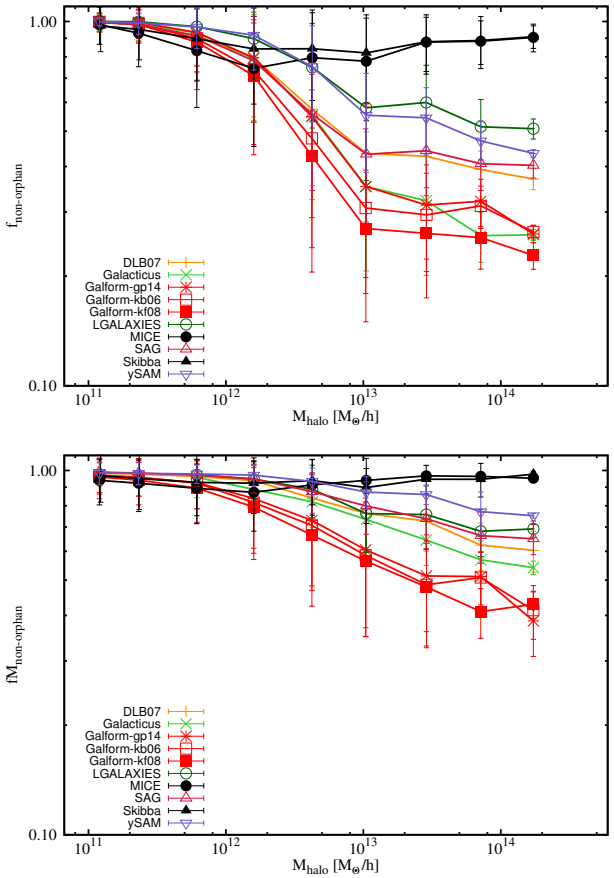

Figure 12. Number fraction (top panel) and stellar mass fraction (bottom panel) of non-orphan galaxies with stellar mass $M_* > 10^9 h^{-1}{\rm M}_\odot$ as a function of main halo mass $M_{\rm halo}$ at redshift $z = 0$. Only models that actually feature orphans are shown here.

is roughly constant for all models although the occupation number of haloes varies between them by around an order of magnitude. While the upper panel of Fig. 14 shows all galaxies – including orphans – the lower panel only shows non-orphan galaxies; we clearly see that the differences between models are primarily due to the (treatment of) orphan galaxies, though significant differences remain even for non-orphans. The difference between the two panels also indicates that orphans are favourably found in higher mass haloes while lower mass objects are practically devoid of them, as already seen in Fig. 12.

The halo occupation distributions (as well as clustering properties) of all the models will be further analyzed in a spin-off project of this collaboration (Pujol et al., in prep.).

7 SUMMARY & DISCUSSION

We have brought together 14 models for galaxy formation in simulations of cosmic structure formation, i.e. 12 SAM and 2 HOD models. In this inaugural paper we presented the models and undertook the first comparison where the models applied their published parameters (without any recalibration) to the same small cosmological volume of $(62.5 h^{-1}{\rm M}_\odot)^3$ with halo merger trees constructed using a single halo finder and tree building algorithm. Hence the framework that underpins this study was designed to be the same

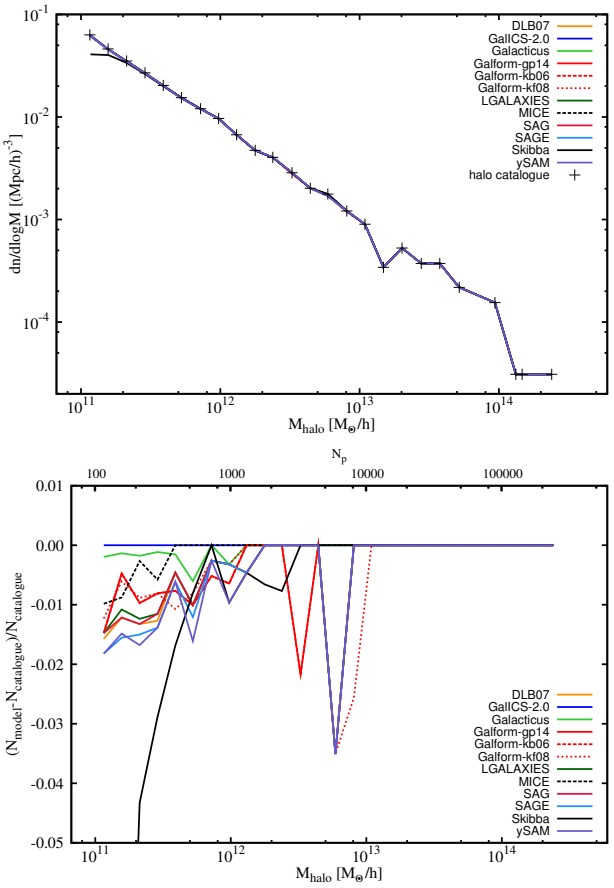

Figure 13. Mass function of all haloes at redshift $z = 0$ as given in the input halo catalogue (crosses, all identified objects down to 20 particles including subhaloes) and as recovered from the non-orphan galaxy catalogues of each model. The upper panel shows the supplied mass function whereas the lower panel shows the fractional difference with respect to the input halo catalogue. The upper panel also gives the translation of $M_{\rm halo}$ to the number of particles in the halo as additional x-axis at the top.

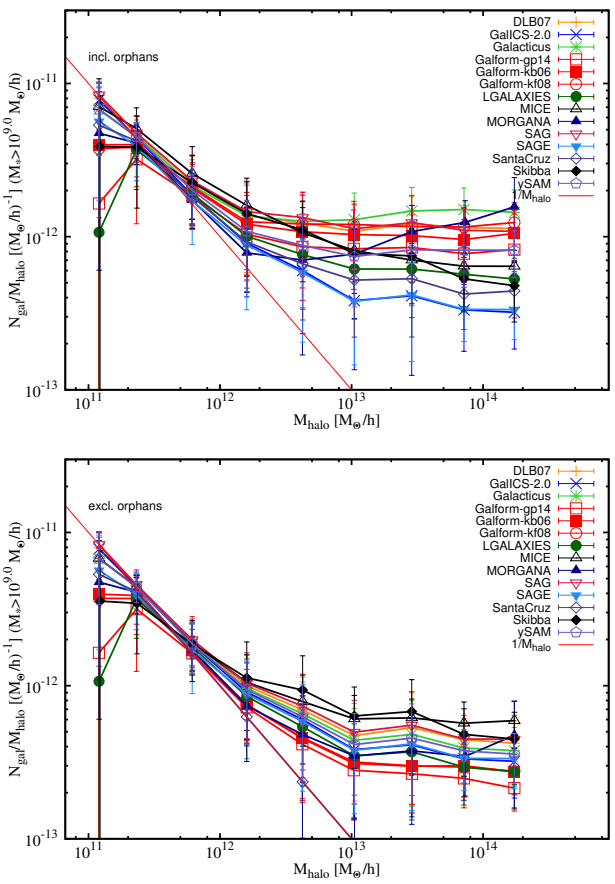

Figure 14. Number of galaxies $N_{\rm gal}$ per halo mass (i.e. 'specific frequency of galaxies') for galaxies more massive than $M_* > 10^9 h^{-1}{\rm M}_\odot$ as a function of halo mass $M_{\rm halo}$ at redshift $z = 0$. Points plotted are the mean values in the bin with respect to both axes and error bars are 1σ. The solid line running from upper left to lower right represents one galaxy per halo. The upper panel shows all galaxies whereas the lower panel focuses on non-orphan galaxies.

for each model. This approach allowed us to directly compare the galaxy formation models themselves leaving aside concerns about cosmic variance, the influence of the halo finder (Avila et al. 2014) or tree construction method (Srisawat et al. 2013; Lee et al. 2014). However, some teams had to slightly alter this framework in order to make the catalogues compatible with the assumptions in their methods (see Appendix A).

All of the contributing teams have been provided with a standardized dark matter halo catalogue and merger tree; they were asked to undertake their currently favoured model and were explicitly told the underlying cosmology and mass resolution of the simulation to be used. They supplied returns in a specified format and the analysis was performed on these files using a single common analysis pipeline. This approach has proved highly successful for other related scientific issues in the past (e.g. Frenk et al. 1999; Heitmann et al. 2008; Knebe et al. 2011; Onions et al. 2012; Srisawat et al. 2013; Kim et al. 2014).

This paper should be viewed as the first in a series emerging out of the nIFTy cosmology workshop[8]. A number of spin-off projects were also initiated at the meeting, including more detailed studies of cold vs. hot gas properties, correlation functions, dust effects, disk instabilities, and – last but not least – how to define a common calibration framework. The results will be presented in future papers.

For the present paper each team applied their published calibration values to the supplied cosmological model as specified in Appendix A which also describes each model's specific choice of parameters. Each team tends to use their own personal preference of which observables to tune their model to, and these observables often require additional processing to produce from the more physically fundamental quantities studied here. For instance, the calculation of luminosities requires the adoption of a particular stellar population synthesis model as well as a certain dust model. Even the derivation of stellar mass demands a choice for the stellar initial mass function. We deliberately deferred from studying magnitudes to avoid the accompanying layer of complexity; and we left the preference for the initial stellar mass function at the modeller's discretion. This choice of calibration freedom was made deliberately in order not to favour any particular model if we happened to make similar (somewhat arbitrary) post-processing choices.

We have explicitly chosen not to overlay our figures with observational data for precisely the same reason: such data requires

[8] http://www.popia.ft.uam.es/nIFTyCosmology

somewhat arbitrary (reverse) conversion from the observed quantities and this conversion may bias the reader in favour of a particular model that happened to convert using the same approach (or happened to tune their model to this particular observational quantity). We reserve such comparisons to future work where we will consider the full range of such conversions and include a careful review of the observational literature on this point. But we nevertheless like to remind the reader that each model has been compared with a variety of observational data and that these comparisons are published.

Given the variety in models and calibrations, the agreement found here is gratifying although a number of discrepancies exist, as summarized here (and discussed below).

Stellar Component The stellar mass functions at $z = 0$ of all the models lie within a range of around a factor of 3 in amplitude across the faint end of the curve and have somewhat different effective breaks at the high mass end. The star formation rate density and specific star formation rate by halo mass is broadly similar for all the SAMs, with the main difference being in normalisation, which can vary by a little under an order of magnitude near the peak of the star formation rate density curve and a factor of three elsewhere.

Galaxies For most of the models considered here, galaxies without a surviving dark matter halo (so-called 'orphan galaxies') dominate the number counts within each host halo, accounting for between 40 and 75 per cent of all galaxies in main haloes above $10^{13}h^{-1}\mathrm{M}_{\odot}$ at redshift $z = 0$. The treatment of these galaxies and their eventual fate differs dramatically between the various models and is also expected to be strongly dependent upon the resolution of the simulation.

Galaxy-Halo Connection All the models populate the supplied trees adequately, i.e. all haloes found in the simulation contain a galaxy. We further found that the specific frequency of galaxies, i.e. the number of galaxies per halo mass, is constant above the completeness limit of the simulation although the average number of galaxies per dark matter halo mass varies by around an order of magnitude across the models, if orphans are included; otherwise the variation is reduced to a factor of about two.

When interpreting the results one needs to always bear in mind that all models were used as originally tuned in the respective reference paper, i.e. the way this comparison has been designed might lead to scatter across models that is larger than the scatter due to different implementations of the same physics within them. The factors entering into the model-to-model variations seen here are differences due to a) models not being tuned to the same observational constraints, b) models being tuned to different cosmologies, c) the choice for the halo mass definition, d) the choice for the applied initial stellar mass function, and e) models not being optimally tuned (for the merger tree structure at hand). Elaborating on these points:

a) observational constraints: Using different observational constraints should not be a primary source of variation, at least as long as constraints for all the relevant physical quantities are included. For instance, the work of Henriques et al. (2013, using SMF+Bband+Kband constraints from $z = 3$ to $z = 0$) and Henriques et al. (2014, using SMF+red fraction constraints) lead to convergent results, if a proper assessment of the observational uncertainties is performed; the authors also state that they need the combination of properties to arrive at converged likelihood regions in parameter space. However, the models included here show an even greater variety of (potentially mutually exclusive) observational constraints and hence we cannot exclude that those differences contribute significantly to the scatter.

b) cosmology: Differences due to cosmology can often (but not always) be absorbed by re-tuning the physical parameters of the model. However, without re-tuning (as here), cosmology can make a big difference; this can be seen, for instance, from the significant changes in parameter values required to get the same stellar mass function at $z = 0$ for different cosmologies (see Wang et al. 2008; Guo et al. 2013; Gonzalez-Perez et al. 2014).

c) halo mass definition: As can be verified in Table 1 another difference across models is the applied definition for halo masses. Furthermore these differences can increase with redshift: for instance, $M_{200\mathrm{c}}$ only depends on the evolution of $\rho_c(z)$ whereas M_{BN98} has an additional dependency on cosmology encoded in the overdensity parameter $\Delta_{\mathrm{BN98}}(z)$. We confirmed that there are variations due to it, but these are not sufficiently large to explain all of the scatter.

d) initial mass function: As for different cosmologies and halo mass definitions, the assumption of different IMFs can be compensated for when calibrating the model: the observational data set used for the calibration (and the initial mass function assumed in its preparation) will determine the values of the model parameters – whatever the assumption for the model IMF. However, the model's stellar masses (and other quantities not studied here such as the recycled fraction of gas, the amount of energy available for supernovae, chemical enrichment, etc.) will certainly be affected by the IMF choice. We can confirm that this has an effect but is not the primary source of the variations between models.

e) tuning: This is by far the most decisive factor for the scatter (Henriques et al. 2009; Mutch et al. 2013). It has been shown by, for instance, Henriques et al. (2009) that DLB07 and an earlier version of the SAGE model could be brought into better agreement with the observational data by re-tuning their parameters optimally. Further, Lee et al. (2014) have shown that differences in merger trees could be overcome by re-tuning the model parameters. This directly applies to the comparison presented here: all models have been designed and tested using different simulations and merger tree (structures), but were not allowed to re-adjust their parameters for this initial project. We have seen that this has a very strong influence on the stellar mass function and is potentially the main source of the scatter seen in the plots throughout this paper. Future papers in this series will investigate the degree to which the models can be brought into agreement, and the extent to which they still differ, once retuned to the same set of observational constraints.

We deliberately did not include any comparison with luminosity-based properties as their calculation involves another layer of complexity, e.g. stellar population synthesis, dust extinction, etc. However – as stated in Appendix A – some models are using luminosity-related quantities to constrain their model parameters. Also, one should not neglect the additional difficulties encountered when moving from intrinsic galaxy properties such as mass to directly observable quantities such as luminosity or colour. Conversely, the stellar mass of a galaxy is not directly observable

and hence any derivation of it relies on modelling itself; therefore – as highlighted a couple of times before already – all observational data comes with its own error estimates that can be as large as 0.5 dex at $z = 0$. All of this will certainly leave its imprint on the models presented here.

8 CONCLUSIONS

We conclude that applying galaxy formation models without due consideration to calibration with respect to cosmology, resolution, and – most importantly – merger tree prescription leads to scatter that could otherwise be avoided (see, e.g. Fontanot et al. 2009; Díaz-Giménez & Mamon 2010; De Lucia et al. 2011; Contreras et al. 2013; Lu et al. 2014; Lee et al. 2014). But the need for recalibration should not be viewed as a flaw of the models: it is a necessary step required to match the model to the particular observational data sets that are chosen to underpin the model. The fact that a good match can be obtained is itself a non-trivial success of the model which indicates that the models capture the underlying key physical phenomena correctly. The (adjusted) parameters then place bounds upon the relevant physics, and the models can be used to test astrophysics outside that used in the calibration step.

We close by mentioning again that this work only forms the initial step in a wider and long overdue programme designed to inter-compare current SAM and HOD models. The next stage is to calibrate all the models to a small, well specified, set of training data, such as for instance the stellar mass function at $z = 0$ and $z = 2$ before re-comparing the models on the other statistics shown in this work. This approach will likely significantly narrow the spread of the returned data on these physical quantities. It will also allow a more detailed comparison on such observationally interesting measures as hot and cold gas fractions, gas metallicity, galaxy sizes and morphologies, etc. The work for this has been started and will form the basis of a future workshop.

ACKNOWLEDGMENTS

The authors would like to express special thanks to the Instituto de Fisica Teorica (IFT-UAM/CSIC in Madrid) for its hospitality and support, via the Centro de Excelencia Severo Ochoa Program under Grant No. SEV-2012-0249, during the three week workshop 'nIFTy Cosmology' where this work developed. We further acknowledge the financial support of the 2014 University of Western Australia Research Collaboration Award for 'Fast Approximate Synthetic Universes for the SKA', the ARC Centre of Excellence for All Sky Astrophysics (CAASTRO) grant number CE110001020, and the two ARC Discovery Projects DP130100117 and DP140100198. We also recognize support from the Universidad Autonoma de Madrid (UAM) for the workshop infrastructure.

AK is supported by the *Ministerio de Economía y Competitividad* (MINECO) in Spain through grant AYA2012-31101 as well as the Consolider-Ingenio 2010 Programme of the *Spanish Ministerio de Ciencia e Innovación* (MICINN) under grant MultiDark CSD2009-00064. He also acknowledges support from the *Australian Research Council* (ARC) grants DP130100117 and DP140100198. He further thanks Nancy Sinatra for the last of the secret agents. PAT acknowledges support from the Science and Technology Facilities Council (grant number ST/L000652/1). FJC acknowledges support from the Spanish Ministerio de Economía y Competitividad project AYA2012-39620. SAC acknowledges grants from CONICET (PIP-220), Argentina. DJC acknowledges receipt of a QEII Fellowship from the Australian Government. PJE is supported by the SSimPL programme and the Sydney Institute for Astronomy (SIfA), DP130100117. FF acknowledges financial contribution from the grants PRIN MIUR 2009 'The Intergalactic Medium as a probe of the growth of cosmic structures' and PRIN INAF 2010 'From the dawn of galaxy formation'. VGP acknowledges support from a European Research Council Starting Grant (DEGAS-259586). This work used the DiRAC Data Centric system at Durham University, operated by the Institute for Computational Cosmology on behalf of the STFC DiRAC HPC Facility (www.dirac.ac.uk). This equipment was funded by BIS National E-infrastructure capital grant ST/K00042X/1, STFC capital grant ST/H008519/1, and STFC DiRAC Operations grant ST/K003267/1 and Durham University. DiRAC is part of the National E-Infrastructure. The work of BH was supported by Advanced Grant 246797 GALFORMOD from the European Research Council. MH acknowledges financial support from the European Research Council via an Advanced Grant under grant agreement no. 321323 NEOGAL. PM has been supported by a FRA2012 grant of the University of Trieste, PRIN2010-2011 (J91J12000450001) from MIUR, and Consorzio per la Fisica di Trieste. NDP was supported by BASAL PFB-06 CATA, and Fondecyt 1150300. Part of the calculations presented here were run using the Geryon cluster at the Center for Astro-Engineering at U. Catolica, which received funding from QUIMAL 130008 and Fondequip AIC-57. CP acknowledges support of the Australian Research Council (ARC) through Future Fellowship FT130100041 and Discovery Project DP140100198. WC and CP acknowledge support of ARC DP130100117. AP was supported by beca FI and 2009-SGR-1398 from Generalitat de Catalunya and project AYA2012-39620 from MICINN. RAS acknowledges support from the NSF grant AST-1055081. RSS thanks the Downsbrough family for their generous support. SKY acknowledges support from the National Research Foundation of Korea (Doyak 2014003730). Numerical simulations were performed using the KISTI supercomputer under the programme of KSC-2013-C3-015.

The authors contributed to this paper in the following ways: AK & FRP formed the core team and wrote the paper (with substantial help from PAT). They also organized week #2 of the nIFTy workshop out of which this work emerged. CS supplied the simulation and halo catalogue for the work presented here. The authors listed in Section A performed the SAM or HOD modelling using their codes, in particular AB, FJC, AC, SC, DC, GDL, FF, VGP, BH, JL, PM, RAS, RS, CVM, and SY actively ran their models with the assistance of JH, MH, and CS. DC and RAS have written Section 3. WC, DC, PJE, CP, and JO assisted with the analysis and data format issues. All authors had the opportunity to proof read and comment on the paper.

This research has made use of NASA's Astrophysics Data System (ADS) and the arXiv preprint server.

REFERENCES

Arrigoni M., Trager S. C., Somerville R. S., Gibson B. K., 2010, MNRAS, 402, 173

Athanassoula E., 2007, MNRAS, 377, 1569

Avila S., Knebe A., Pearce F. R., Schneider A., Srisawat C., Thomas P. A., Behroozi P., Elahi P. J., Han J., Mao Y.-Y., Onions J., Rodriguez-Gomez V., Tweed D., 2014, MNRAS, 441, 3488

Baldry I. K., Driver S. P., Loveday J., Taylor E. N., Kelvin L. S., Liske J., Norberg P., Robotham A. S. G., et al. 2012, MNRAS, 421, 621
Battin R. H., 1987, An introduction to the mathematics and methods of astrodynamics.
Baugh C. M., 2006, Rep. Prog. Phys., 69, 3101
Behroozi P. S., Wechsler R. H., Conroy C., 2013, ApJ, 770, 57
Bell E. F., de Jong R. S., 2001, ApJ, 550, 212
Benson A. J., 2012, New A, 17, 175
Benson A. J., 2014, MNRAS, 444, 2599
Benson A. J., Babul A., 2009, MNRAS, 397, 1302
Benson A. J., Pearce F. R., Frenk C. S., Baugh C. M., Jenkins A., 2001, MNRAS, 320, 261
Berlind A. A., Weinberg D. H., 2002, ApJ, 575, 587
Bernardi M., Meert A., Sheth R. K., Vikram V., Huertas-Company M., Mei S., Shankar F., 2013, MNRAS, 436, 697
Bernyk M., Croton D. J., Tonini C., Hodkinson L., Hassan A. H., Garel T., Duffy A. R., Mutch S. J., Poole G. B., 2014, ArXiv e-prints
Bigiel F., Leroy A., Walter F., Brinks E., de Blok W. J. G., Madore B., Thornley M. D., 2008, AJ, 136, 2846
Binney J., Tremaine S., 1987, Galactic dynamics. Princeton, NJ, Princeton University Press, 1987, 747 p.
Binney J., Tremaine S., 2008, Galactic Dynamics: Second Edition. Princeton University Press
Blanchard A., Valls-Gabaud D., Mamon G. A., 1992, A&A, 264, 365
Blanton M. R., Eisenstein D., Hogg D. W., Schlegel D. J., Brinkmann J., 2005, ApJ, 629, 143
Blanton M. R., et al. 2003, ApJ, 592, 819
Blanton M. R., Lupton R. H., Schlegel D. J., Strauss M. A., Brinkmann J., Fukugita M., Loveday J., 2005a, ApJ, 631, 208
Blanton M. R., Lupton R. H., Schlegel D. J., Strauss M. A., Brinkmann J., Fukugita M., Loveday J., 2005b, ApJ, 631, 208
Blumenthal G. R., Faber S. M., Flores R., Primack J. R., 1986, ApJ, 301, 27
Bond J. R., Cole S., Efstathiou G., Kaiser N., 1991, ApJ, 379, 440
Bondi H., 1952, MNRAS, 112, 195
Bower R. G., Benson A. J., Malbon R., Helly J. C., Frenk C. S., Baugh C. M., Cole S., Lacey C. G., 2006, MNRAS, 370, 645
Boylan-Kolchin M., Ma C.-P., Quataert E., 2008, MNRAS, 383, 93
Bryan G. L., Norman M. L., 1998, ApJ, 495, 80
Carretero J., Castander F. J., Gaztañaga E., Crocce M., Fosalba P., 2015, MNRAS, 447, 646
Castander F. J., Carretero J., Crocce M., Fosalba P., Gaztanaga E., 2014, in preparation
Cattaneo A., Blaizot J., Weinberg D. H., Kereš D., Colombi S., Davé R., Devriendt J., Guiderdoni B., Katz N., 2007, MNRAS, 377, 63
Cattaneo A., Dekel A., Devriendt J., Guiderdoni B., Blaizot J., 2006, MNRAS, 370, 1651
Cattaneo A., Faber S. M., Binney J., Dekel A., Kormendy J., Mushotzky R., Babul A., Best P. N., Brüggen M., Fabian A. C., Frenk C. S., Khalatyan A., Netzer H., Mahdavi A., Silk J., Steinmetz M., Wisotzki L., 2009, Nature, 460, 213
Cattaneo A., Mamon G. A., Warnick K., Knebe A., 2011, A&A, 533, A5
Cattaneo A., Teyssier R., 2007, MNRAS, 376, 1547
Cavaliere A., Fusco-Femiano R., 1976, A&A, 49, 137
Chabrier G., 2003, PASP, 115, 763
Chandrasekhar S., 1943, ApJ, 97, 255
Cole S., 1991, ApJ, 367, 45
Cole S., Lacey C. G., Baugh C. M., Frenk C. S., 2000, MNRAS, 319, 168
Cole S., Norberg P., Baugh C. M., Frenk C. S., Bland-Hawthorn J., Bridges T., Cannon R., Colless M., Collins C., Couch W., Cross N., Dalton G., De Propris R., Driver S. P., 2001, Monthly Notices of the Royal Astronomical Society, 326, 255
Conroy C., Wechsler R. H., Kravtsov A. V., 2006, ApJ, 647, 201
Contreras S., Baugh C. M., Norberg P., Padilla N., 2013, MNRAS, 432, 2717
Cooray A., Sheth R., 2002, Phys. Rep., 372, 1
Cora S. A., 2006, MNRAS, 368, 1540
Covington M. D., Primack J. R., Porter L. A., Croton D. J., Somerville R. S., Dekel A., 2011, MNRAS, 415, 3135
Cox T. J., Jonsson P., Somerville R. S., Primack J. R., Dekel A., 2008, MNRAS, 384, 386
Cox T. J., Primack J., Jonsson P., Somerville R. S., 2004, ApJ, 607, L87
Crocce M., Castander F. J., Gaztanaga E., Fosalba P., Carretero J., 2013, ArXiv e-prints
Croton D. J., Springel V., White S. D. M., De Lucia G., Frenk C. S., Gao L., Jenkins A., Kauffmann G., Navarro J. F., Yoshida N., 2006, MNRAS, 365, 11
Davis M., Efstathiou G., Frenk C. S., White S. D. M., 1985, ApJ, 292, 371
de Jong R. S., Lacey C., 2000, The Astrophysical Journal, 545, 781
De Lucia G., Blaizot J., 2007a, MNRAS, 375, 2
De Lucia G., Blaizot J., 2007b, MNRAS, 375, 2
De Lucia G., Boylan-Kolchin M., Benson A. J., Fontanot F., Monaco P., 2010, MNRAS, 406, 1533
De Lucia G., Fontanot F., Wilman D., Monaco P., 2011, MNRAS, 414, 1439
De Lucia G., Kauffmann G., White S. D. M., 2004a, MNRAS, 349, 1101
De Lucia G., Kauffmann G., White S. D. M., 2004b, MNRAS, 349, 1101
Dekel A., Birnboim Y., 2006, MNRAS, 368, 2
Dekel A., Birnboim Y., Engel G., Freundlich J., Goerdt T., Mumcuoglu M., Neistein E., Pichon C., Teyssier R., Zinger E., 2009, Nature, 457, 451
Dekel A., Silk J., 1986, ApJ, 303, 39
Díaz-Giménez E., Mamon G. A., 2010, MNRAS, 409, 1227
Driver S. P., Robotham A. S. G., Kelvin L., Alpaslan M., Baldry I. K., Bamford S. P., Brough S., Brown M., et al. 2012, MNRAS, 427, 3244
Efstathiou G., Lake G., Negroponte J., 1982, MNRAS, 199, 1069
Ferland G. J., Porter R. L., van Hoof P. A. M., Williams R. J. R., Abel N. P., Lykins M. L., Shaw G., Henney W. J., Stancil P. C., 2013, Rev. Mexicana Astron. Astrofis., 49, 137
Font A. S., Bower R. G., McCarthy I. G., Benson A. J., Frenk C. S., Helly J. C., Lacey C. G., Baugh C. M., Cole S., 2008, MNRAS, 389, 1619
Fontanot F., Cristiani S., Santini P., Fontana A., Grazian A., Somerville R. S., 2012, MNRAS, 421, 241
Fontanot F., De Lucia G., Monaco P., Somerville R. S., Santini P., 2009, MNRAS, 397, 1776
Fontanot F., De Lucia G., Wilman D., Monaco P., 2011, MNRAS, 416, 409
Fosalba P., Crocce M., Gaztañaga E., Castander F. J., 2013, ArXiv e-prints
Fosalba P., Gaztanaga E., Castander F. J., Crocce M., 2013, ArXiv

e-prints
Foster A. R., Ji L., Smith R. K., Brickhouse N. S., 2012, ApJ, 756, 128
Frenk C. S., White S. D. M., 2012, Annalen der Physik, 524, 507
Frenk et al. C. S., 1999, ApJ, 525, 554
Fu J., Kauffmann G., Huang M.-l., Yates R. M., Moran S., Heckman T. M., Davé R., Guo Q., Henriques B. M. B., 2013, MNRAS, 434, 1531
Gallazzi A., Charlot S., Brinchmann J., White S. D. M., Tremonti C. A., 2005, MNRAS, 362, 41
Gao L., De Lucia G., White S. D. M., Jenkins A., 2004, MNRAS, 352, L1
Gargiulo I. D., Cora S. A., Padilla N. D., Muñoz Arancibia A. M., Ruiz A. N., Orsi A. A., Tecce T. E., Weidner C., Bruzual G., 2014, ArXiv e-prints
Gill S. P. D., Knebe A., Gibson B. K., 2004, MNRAS, 351, 399
Gill S. P. D., Knebe A., Gibson B. K., 2005, MNRAS, 356, 1327
Gnedin O. Y., Kravtsov A. V., Klypin A. A., Nagai D., 2004, ApJ, 616, 16
Gonzalez-Perez V., Lacey C. G., Baugh C. M., Lagos C. D. P., Helly J., Campbell D. J. R., Mitchell P. D., 2014, MNRAS, 439, 264
Guo Q., White S., Angulo R. E., Henriques B., Lemson G., Boylan-Kolchin M., Thomas P., Short C., 2013, MNRAS, 428, 1351
Guo Q., White S., Boylan-Kolchin M., De Lucia G., Kauffmann G., Lemson G., Li C., Springel V., Weinmann S., 2011, MNRAS, 413, 101
Guo Q., White S., Li C., Boylan-Kolchin M., 2010, MNRAS, 404, 1111
Hansen S. M., Sheldon E. S., Wechsler R. H., Koester B. P., 2009, ApJ, 699, 1333
Häring N., Rix H.-W., 2004, Astrophysical Journal, 604, L89
Häring N., Rix H.-W., 2004, ApJL, 604, L89
Hatton S., Devriendt J. E. G., Ninin S., Bouchet F. R., Guiderdoni B., Vibert D., 2003, MNRAS, 343, 75
Hearin A. P., Watson D. F., 2013, MNRAS, 435, 1313
Heitmann K., Lukić Z., Fasel P., Habib S., Warren M. S., White M., Ahrens J., Ankeny L., Armstrong R., O'Shea B., Ricker P. M., Springel V., Stadel J., Trac H., 2008, Computational Science and Discovery, 1, 015003
Helly J. C., Cole S., Frenk C. S., Baugh C. M., Benson A., Lacey C., Pearce F. R., 2003, MNRAS, 338, 913
Henriques B., White S., Thomas P., Angulo R., Guo Q., de Lucia G., Kauffmann G., Lemson G., Springel V., 2014, in preparation
Henriques B., White S., Thomas P., Angulo R., Guo Q., Lemson G., Springel V., Overzier R., 2014, ArXiv e-prints
Henriques B. M. B., Thomas P. A., Oliver S., Roseboom I., 2009, MNRAS, 396, 535
Henriques B. M. B., White S. D. M., Thomas P. A., Angulo R. E., Guo Q., Lemson G., Springel V., 2013, MNRAS, 431, 3373
Hirschi R., Meynet G., Maeder A., 2005, A&A, 433, 1013
Hirschmann M., Naab T., Somerville R. S., Burkert A., Oser L., 2012, MNRAS, 419, 3200
Hirschmann M., Somerville R. S., Naab T., Burkert A., 2012, MNRAS, 426, 237
Hoffmann K., Bel J., Gaztañaga E., Crocce M., Fosalba P., Castander F. J., 2015, MNRAS, 447, 1724
Hopkins A. M., 2004, Astrophysical Journal, 615, 209
Hopkins P. F., Somerville R. S., Cox T. J., Hernquist L., Jogee S., Kereš D., Ma C.-P., Robertson B., Stewart K., 2009, MNRAS, 397, 802
Ilbert O., et al. 2009, ApJ, 690, 1236
Ilbert O., McCracken H. J., Le Fèvre O., Capak P., Dunlop J., Karim A., Renzini M. A., Caputi K., et al. 2013, A&A, 556, A55
Iwamoto K., Brachwitz F., Namoto K., Kishimoto N., Umeda H., Hix W. R., Thielemann F., 1999, ApJS, 125, 439
Jiang C. Y., Jing Y. P., Faltenbacher A., Lin W. P., Li C., 2008, ApJ, 675, 1095
Jiang L., Helly J. C., Cole S., Frenk C. S., 2014, MNRAS, 440, 2115
Jing Y. P., Mo H. J., Boerner G., 1998, ApJ, 494, 1
Karakas A. I., 2010, MNRAS, 403, 1413
Kauffmann G., 1996, MNRAS, 281, 475
Kauffmann G., Colberg J. M., Diaferio A., White S. D. M., 1999, MNRAS, 303, 188
Kauffmann G., Haehnelt M., 2000, MNRAS, 311, 576
Kauffmann G., White S. D. M., Guiderdoni B., 1993, MNRAS, 264, 201
Kennicutt Jr. R. C., 1983, ApJ, 272, 54
Kennicutt Jr. R. C., 1998, in G. Gilmore & D. Howell ed., The Stellar Initial Mass Function (38th Herstmonceux Conference) Vol. 142 of Astronomical Society of the Pacific Conference Series, Overview: The Initial Mass Function in Galaxies. pp 1–+
Kim J.-h., Abel T., Agertz O., Bryan G. L., Ceverino D., Christensen C., Conroy C., Dekel A., AGORA Collaboration29 f. t., 2014, ApJS, 210, 14
Kimm T., Somerville R. S., Yi S. K., van den Bosch F. C., Salim S., Fontanot F., Monaco P., Mo H., Pasquali A., Rich R. M., Yang X., 2009, MNRAS, 394, 1131
Kimm T., Yi S. K., Khochfar S., 2011, ApJ, 729, 11
Klypin A. A., Trujillo-Gomez S., Primack J., 2011, ApJ, 740, 102
Knebe A., Knollmann S. R., Muldrew S. I., Pearce F. R., et al. 2011, MNRAS, 415, 2293
Knollmann S. R., Knebe A., 2009, ApJS, 182, 608
Kobayashi C., Umeda H., Nomoto K., Tominaga N., Ohkubo T., 2006, ApJ, 653, 1145
Kochanek C. S., Pahre M. A., Falco E. E., Huchra J. P., Mader J., Jarrett T. H., Chester T., Cutri R., Schneider S. E., 2001, ApJ, 560, 566
Komatsu E., Smith K. M., Dunkley J., Bennett C. L., Gold B., Hinshaw G., Jarosik N., Larson D., Nolta M. R., Page L., Spergel D. N., Halpern M., Hill R. S., Kogut A., Limon M., Meyer S. S., Odegard N., Tucker G. S., Weiland J. L., Wollack E., 2011, ApJS, 192, 18
Krumholz M. R., McKee C. F., Tumlinson J., 2009, ApJ, 699, 850
Lacey C., Cole S., 1993, MNRAS, 262, 627
Lacey C., Silk J., 1991, ApJ, 381, 14
Lagos C., Cora S., Padilla N. D., 2008, MNRAS, 388, 587
Lagos C. D. P., Baugh C. M., Lacey C. G., Benson A. J., Kim H.-S., Power C., 2011, MNRAS, 418, 1649
Lee J., Yi S. K., 2013, ApJ, 766, 38
Lee J., Yi S. K., Elahi P. J., Thomas P. A., Pearce F. R., Behroozi P., Han J., Helly J., Jung I., Knebe A., Mao Y.-Y., Onions J., Rodriguez-Gomez V., Schneider A., Srisawat C., Tweed D., 2014, ArXiv e-prints
Li C., White S. D. M., 2009, Monthly Notices of the Royal Astronomical Society, 398, 2177
Lia C., Portinari L., Carraro G., 2002, MNRAS, 330, 821
Lo Faro B., Monaco P., Vanzella E., Fontanot F., Silva L., Cristiani S., 2009, MNRAS, 399, 827
Lu Y., Kereš D., Katz N., Mo H. J., Fardal M., Weinberg M. D., 2011, MNRAS, 416, 660

Lu Y., Wechsler R. H., Somerville R. S., Croton D., Porter L., Primack J., Behroozi P. S., Ferguson H. C., Koo D. C., Guo Y., Safarzadeh M., Finlator K., Castellano M., White C. E., Sommariva V., Moody C., 2014, ApJ, 795, 123
Macciò A. V., Dutton A. A., van den Bosch F. C., 2008, MNRAS, 391, 1940
Macciò A. V., Kang X., Fontanot F., Somerville R. S., Koposov S., Monaco P., 2010, MNRAS, 402, 1995
Madau P., Dickinson M., 2014, ARA&A, 52, 415
Marigo P., 2001, A&A, 370, 194
McCarthy I. G., Frenk C. S., Font A. S., Lacey C. G., Bower R. G., Mitchell N. L., Balogh M. L., Theuns T., 2008, MNRAS, 383, 593
Melinder J., Dahlen T., Mencía Trinchant L., stlin G., Mattila S., Sollerman J., Fransson C., Hayes M., Kankare E., Nasoudi-Shoar S., 2012, A&A, 545, 96
Mihos J. C., Hernquist L., 1994a, ApJ, 425, L13
Mihos J. C., Hernquist L., 1994b, ApJ, 431, L9
Mihos J. C., Hernquist L., 1996, ApJ, 464, 641
Mitchell P. D., Lacey C. G., Baugh C. M., Cole S., 2013, MNRAS, 435, 87
Mo H. J., Mao S., White S. D. M., 1998, MNRAS, 295, 319
Monaco P., 2004, MNRAS, 352, 181
Monaco P., Benson A. J., De Lucia G., Fontanot F., Borgani S., Boylan-Kolchin M., 2014, MNRAS, 441, 2058
Monaco P., Fontanot F., Taffoni G., 2007, MNRAS, 375, 1189
Monaco P., Theuns T., Taffoni G., 2002, MNRAS, 331, 587
More S., van den Bosch F. C., Cacciato M., Skibba R., Mo H. J., Yang X., 2011, MNRAS, 410, 210
Moster B. P., Somerville R. S., Maulbetsch C., van den Bosch F. C., Macciò A. V., Naab T., Oser L., 2010, ApJ, 710, 903
Moustakas J., Coil A. L., Aird J., Blanton M. R., Cool R. J., Eisenstein D. J., Mendez A. J., Wong K. C., Zhu G., Arnouts S., 2013, ApJ, 767, 50
Muñoz-Cuartas J. C., Macciò A. V., Gottlöber S., Dutton A. A., 2011, MNRAS, 411, 584
Muldrew S. I., Pearce F. R., Power C., 2011, MNRAS, 410, 2617
Munari E., Biviano A., Borgani S., Murante G., Fabjan D., 2013, MNRAS, 430, 2638
Mutch S. J., Poole G. B., Croton D. J., 2013, MNRAS, 428, 2001
Navarro J. F., Frenk C. S., White S. D. M., 1997, ApJ, 490, 493
Nelson C. J., Shelyag S., Mathioudakis M., Doyle J. G., Madjarska M. S., Uitenbroek H., Erdélyi R., 2013, ApJ, 779, 125
Nomoto K., Thielemann F.-K., Wheeler J. C., 1984, ApJ, 279, L23
Norberg P., Cole S., Baugh C. M., Frenk C. S., Baldry I., Bland-Hawthorn J., Bridges T., Cannon R., et al. 2002, Monthly Notices of the Royal Astronomical Society, 336, 907
Norberg P., Cole S., Baugh C. M., Frenk C. S., Baldry I., Bland-Hawthorn J., Bridges T., Cannon R., et al. 2002, MNRAS, 336, 907
Ocvirk P., Pichon C., Teyssier R., 2008, MNRAS, 390, 1326
Onions J., Knebe A., Pearce F. R., Muldrew S. I., Lux H., Knollmann S. R., Ascasibar Y., Behroozi P., Elahi P., Han J., Maciejewski M., Merchán M. E., Neyrinck M., Ruiz A. N., Sgró M. A., Springel V., Tweed D., 2012, MNRAS, p. 2881
Orsi Á., Padilla N., Groves B., Cora S., Tecce T., Gargiulo I., Ruiz A., 2014, MNRAS, 443, 799
Oser L., Naab T., Ostriker J. P., Johansson P. H., 2012, ApJ, 744, 63
Padilla N. D., Salazar-Albornoz S., Contreras S., Cora S. A., Ruiz A. N., 2014, MNRAS, 443, 2801
Padovani P., Matteucci F., 1993, ApJ, 416, 26
Panter B., Jimenez R., Heavens A. F., Charlot S., 2008, MNRAS, 391, 1117
Parkinson H., Cole S., Helly J., 2008, MNRAS, 383, 557
Pipino A., Devriendt J. E. G., Thomas D., Silk J., Kaviraj S., 2009, A&A, 505, 1075
Pizagno J., Prada F., Weinberg D. H., Rix H.-W., Pogge R. W., Grebel E. K., Harbeck D., Blanton M., Brinkmann J., Gunn J. E., 2007, Astronomical Journal, 134, 945
Porter L. A., Somerville R. S., Primack J. R., Johansson P. H., 2014, ArXiv e-prints, 1407.0594, MNRAS in press
Portinari L., Chiosi C., Bressan A., 1998, A&A, 334, 505
Press W. H., Schechter P., 1974, ApJ, 187, 425
Roukema B. F., Quinn P. J., Peterson B. A., Rocca-Volmerange B., 1997, MNRAS, 292, 835
Ruiz A. N., Cora S. A., Padilla N. D., Domínguez M. J., Vega-Martínez C. A., Tecce T. E., Orsi Á., Yaryura Y., García Lambas D., Gargiulo I. D., Muñoz Arancibia A. M., 2015, ApJ, 801, 139
Sani E., Lutz D., Risaliti G., Netzer H., Gallo L. C., Trakhtenbrot B., Sturm E., Boller T., 2010, MNRAS, 403, 1246
Saro A., De Lucia G., Borgani S., Dolag K., 2010, MNRAS, 406, 729
Schaye J., Crain R. A., Bower R. G., Furlong M., Schaller M., Theuns T., Dalla Vecchia C., Frenk C. S., et al. 2015, MNRAS, 446, 521
Scoccimarro R., Sheth R. K., Hui L., Jain B., 2001, ApJ, 546, 20
Shankar F., Marulli F., Bernardi M., Mei S., Meert A., Vikram V., 2013, MNRAS, 428, 109
Shankar F., Mei S., Huertas-Company M., Moreno J., Fontanot F., Monaco P., Bernardi M., Cattaneo A., Sheth R., Licitra R., Delaye L., Raichoor A., 2014, MNRAS, 439, 3189
Skibba R., Sheth R. K., Connolly A. J., Scranton R., 2006, MNRAS, 369, 68
Skibba R. A., Macciò A. V., 2011, MNRAS, 416, 2388
Skibba R. A., Sheth R. K., 2009, MNRAS, 392, 1080
Skibba R. A., van den Bosch F. C., Yang X., More S., Mo H., Fontanot F., 2011, MNRAS, 410, 417
Snaith O. N., Gibson B. K., Brook C. B., Courty S., Sánchez-Blázquez P., Kawata D., Knebe A., Sales L. V., 2011, MNRAS, 415, 2798
Somerville R. S., Barden M., Rix H.-W., Bell E. F., Beckwith S. V. W., Borch A., Caldwell J. A. R., Häußler B., Heymans C., Jahnke K., Jogee S., McIntosh D. H., Meisenheimer K., Peng C. Y., Sánchez S. F., Wisotzki L., Wolf C., 2008, ApJ, 672, 776
Somerville R. S., Davé R., 2014, ArXiv e-prints
Somerville R. S., Gilmore R. C., Primack J. R., Domínguez A., 2012, MNRAS, 423, 1992
Somerville R. S., Hopkins P. F., Cox T. J., Robertson B. E., Hernquist L., 2008, MNRAS, 391, 481
Somerville R. S., Kolatt T. S., 1999, MNRAS, 305, 1
Somerville R. S., Primack J. R., 1999, MNRAS, 310, 1087
Somerville R. S., Primack J. R., Faber S. M., 2001, MNRAS, 320, 504
Springel V., 2005, MNRAS, 364, 1105
Springel V., White S. D. M., Jenkins A., Frenk C. S., Yoshida N., Gao L., Navarro J., Thacker R., Croton D., Helly J., Peacock J. A., Cole S., Thomas P., Couchman H., Evrard A., Colberg J., Pearce F., 2005, Nature, 435, 629
Springel V., White S. D. M., Tormen G., Kauffmann G., 2001a, MNRAS, 328, 726
Springel V., White S. D. M., Tormen G., Kauffmann G., 2001b, MNRAS, 328, 726
Springel V., Yoshida N., White S. D. M., 2001, New Astronomy,

6, 79
Srisawat C., Knebe A., Pearce F. R., Schneider A., Thomas P. A., Behroozi P., Dolag K., Elahi P. J., Han J., Helly J., Jing Y., Jung I., Lee J., Mao Y.-Y., Onions J., Rodriguez-Gomez V., Tweed D., Yi S. K., 2013, MNRAS, 436, 150
Sutherland R. S., Dopita M. A., 1993, ApJS, 88, 253
Taffoni G., Mayer L., Colpi M., Governato F., 2003, MNRAS, 341, 434
Tasitsiomi A., Kravtsov A. V., Wechsler R. H., Primack J. R., 2004, ApJ, 614, 533
Tecce T. E., Cora S. A., Tissera P. B., Abadi M. G., Lagos C. D. P., 2010, MNRAS, 408, 2008
Thomas D., Maraston C., Schawinski K., Sarzi M., Silk J., 2010, MNRAS, 404, 1775
Tremonti C. A., Heckman T. M., Kauffmann G., Brinchmann J., Charlot S., White S. D. M., Seibert M., Peng E. W., Schlegel D. J., Uomoto A., Fukugita M., Brinkmann J., 2004, ApJ, 613, 898
Tundo E., Bernardi M., Hyde J. B., Sheth R. K., Pizzella A., 2007, ApJ, 663, 53
Vale A., Ostriker J. P., 2004, MNRAS, 353, 189
van den Bosch F. C., Aquino D., Yang X., Mo H. J., Pasquali A., McIntosh D. H., Weinmann S. M., Kang X., 2008, MNRAS, 387, 79
Viola M., Monaco P., Borgani S., Murante G., Tornatore L., 2008, MNRAS, 383, 777
Vogelsberger M., Genel S., Springel V., Torrey P., Sijacki D., Xu D., Snyder G., Bird S., Nelson D., Hernquist L., 2014, Nature, 509, 177
Wang J., De Lucia G., Kitzbichler M. G., White S. D. M., 2008, MNRAS, 384, 1301
Weinmann S. M., van den Bosch F. C., Yang X., Mo H. J., 2006, Monthly Notices of the Royal Astronomical Society, 366, 2
White S. D. M., Frenk C. S., 1991, ApJ, 379, 52
White S. D. M., Rees M. J., 1978, MNRAS, 183, 341
Yang X., Mo H. J., van den Bosch F. C., 2003, MNRAS, 339, 1057
Yang X., Mo H. J., van den Bosch F. C., 2009, ApJ, 695, 900
Yang X., Mo H. J., van den Bosch F. C., Zhang Y., Han J., 2012, ApJ, 752, 41
Yates R. M., Henriques B., Thomas P. A., Kauffmann G., Johansson J., White S. D. M., 2013, MNRAS, 435, 3500
Yi S. K., Lee J., Jung I., Ji I., Sheen Y.-K., 2013, A&A, 554, A122
York D. G., et al. 2000, AJ, 120, 1579
Yoshida N., Stoehr F., Springel V., White S. D. M., 2002, MNRAS, 335, 762
Zehavi I., Zheng Z., Weinberg D. H., Blanton M. R., Bahcall N. A., Berlind A. A., Brinkmann J., Frieman J. A., Gunn J. E., Lupton R. H., Nichol R. C., Percival W. J., Schneider D. P., Skibba R. A., Strauss M. A., Tegmark M., York D. G., 2011, ApJ, 736, 59
Zibetti S., Charlot S., Rix H.-W., 2009, MNRAS, 400, 1181

APPENDIX A: GALAXY FORMATION MODELS

A1 GALACTICUS (Benson)

The GALACTICUS semi-analytic galaxy formation code (Benson 2012) was designed to be highly modular. Every physical process is implemented through a simple and well-defined interface into which an alternative implementation of a calculation can easily be added. Similarly, the physical description of galaxies is extremely flexible. Each galaxy has a set of components (e.g. disk, dark matter halo, super-massive black hole, etc.) which can be created/destroyed as needed, each of which has a set of properties. The formation and evolution of galaxies is treated by simply defining a set of differential equations for each galaxy. These are all simply fed in to an ordinary differential equation (ODE) solver which evolves them to a specified accuracy, removing any need for fixed timesteps. When running on merger trees derived from N-body simulations, halo masses are interpolated linearly in time between available snapshots. In addition to this differential evolution galaxy components can define 'interrupts' so that the ODE solver stops, allowing the creation of new components (e.g. the first time gas cools and infalls it needs to create a disk component) or to handle discrete events (e.g. if a merger occurs the ODE solver is interrupted, the merger processed, and then the ODE solver starts up again).

Cooling Cooling rates from the hot halo are computed using the traditional cooling radius approach (White & Frenk 1991), with a time available for cooling equal to the halo dynamical time, and assuming a β-model profile with isothermal temperature profile (at the virial temperature). Metallicity dependent cooling curves are computed using CLOUDY (v13.01, Ferland et al. 2013) assuming collisional ionization equilbrium.

Star formation Star formation in disks is modeled using the prescription of Krumholz et al. (2009), assuming that the cold gas of each galaxy is distributed with an exponential radial distribution. The scale length of this distribution is computed from the disks angular momentum by solving for the equilibrium radius within the gravitational potential of the disk+bulge+dark matter halo system (accounting for adiabatic contraction using the algorithm of Gnedin et al. 2004).

Initial mass function A Chabrier (2003) IMF is used throughout.

Metal treatment Metal enrichment is followed using the instantaneous recycling approximation, with a recycled fraction of 0.46 and yield of 0.035. Metals are assumed to be fully mixed in all phases, and so trace all mass flows between phases. Metals affect the cooling rates from the hot halo, and also the star formation rate in disks (Krumholz et al. 2009).

Supernova feedback and winds The wind mass loading factor, β, is computed as $\beta = (V_{\rm disk}/250{\rm km/s})^{-3.5}$ where $V_{\rm disk}$ is the circular velocity at the disk scale radius. Winds move cold gas from the disk back into the hot halo, where it remains in an outflowed phase for some time before being reincorporated and possibly cooling once again. In the case of satellite galaxies, the ouflowing gas is added to the hot halo of the satellite's host.

Gas ejection & reincorporation Gas removed from galaxies by winds is retained in an outflowed reservoir. This reservoir gradually leaks mass back into the hot halo on a timescale of $t_{\rm dyn}/5$ where $t_{\rm dyn}$ is the dynamical time of the halo at the virial radius.

Disk instability The Efstathiou et al. (1982) criterion is used to judge when disks are unstable, with a stability threshold that depends on the gas fraction in the disk (0.7 for pure gas disks, 1.1

for pure stellar, linearly interpolated in between). When a disk is unstable, it begins to transfer stars and gas from the disk to the bulge on a timescale that equals the disk dynamical time for a maximally unstable disk, and increases to infinite timescale as the disk approaches the stability threshold.

Starburst There is no special "starburst" mode in GALACTICUS. Instead, gas in the spheroid forms stars at a rate $\dot{M}_\star = 0.04 M_{\rm gas}/t_{\rm dyn}(V/200{\rm km/s})^{-2}$, where $t_{\rm dyn}$ is the dynamical time of the spheroid at its half mass radius, and V its circular velocity at the same radius. Starburst-level star formation rates are reached if enough gas is deposited into the spheroid, such as happens after a merger.

AGN feedback The mass and spin of black holes are followed in detail, assuming black holes accrete from both the hot halo and spheroid gas. When black holes are accreting from an advection dominated accretion flow, we compute the power of the jet produced by the black hole using the method of Benson & Babul (2009). This jet power is used to offset the cooling luminosity in the hot halo (if, and only if, the hot halo is in a hydrostatic phase), thereby reducing the cooling rate onto the galaxy. Additionally, a radiatively-driven wind is launched from the spheroid by the black hole, assuming that a fraction 0.0024 of its radiative output couples efficiently to the outflow.

Merger treatment A merger between two galaxies is deemed to be "major" if their mass ratio exceeds 1:4. In major mergers, the stars and gas of the two merging galaxies are rearranged into a spheroidal remnant. In other, minor mergers, the merging galaxy is added to the spheroid of the galaxy that it merges with, while the disk of that galaxy is left unaffected.

Substructures Substructures are traced using the subhalo information from the N-body simulation.

Orphans When a subhalo can no longer be found in the N-body merger trees, a "subresolution merging time" is computed for the subhalo (based on its last known orbital properties and the algorithm of Boylan-Kolchin et al. (2008) algorithm. The associated galaxy is then an orphan, which continues to evolve as normal (although we have no detailed knowledge of its position within its host halo) until the subresolution merging time has passed, as which point it is assumed to merge with the central galaxy of its host halo.

Calibration method The parameters of galaxy formation physics in GALACTICUS have been chosen by manually searching parameter space and seeking models which provide a reasonable match to a variety of observational data, including the $z = 0$ stellar mass function of galaxies (Li & White 2009), $z = 0$ K and b_J-band luminosity functions (Cole et al. 2001; Norberg et al. 2002), the local Tully-Fisher relation (Pizagno et al. 2007), the color-magnitude distribution of galaxies in the local Universe (Weinmann et al. 2006), the distribution of disk sizes at $z = 0$ (de Jong & Lacey 2000), the black hole mass–bulge mass relation (Häring & Rix 2004), and the star formation history of the Universe (Hopkins 2004). GALACTICUS has also been calibrated to the local stellar mass function using MCMC techniques (Benson 2014), but so far only for a simplified implementation of galaxy formation physics. As such, we do not use this MCMC-calibrated version of GALACTICUS here.

Model origin The parameters used were calibrated using Monte Carlo trees built using the algorithm of Parkinson et al. (2008).

Modifications to the supplied data When importing merger trees for this project, GALACTICUS aims to make minimal changes to the tree structure. Two small modifications are required to ensure consistency of the merger trees. First, where halo A is indicated as being the host of halo B, but A is not present in the merger trees (i.e. is not listed as the progenitor of any other halo), then A is assumed to be a progenitor of the same halo of which B is a progenitor. Second, if two haloes are mutual hosts (i.e. A is the host of B, while B is the host of A), GALACTICUS resolves this inconsistency by reassigning the more massive of the two haloes to be unhosted (i.e. to no longer be classified as a subhalo). No further modifications are made. In particular, this means that subhalo-subhalo mergers are allowed, subhaloes are allowed to become non-subhaloes later in their evolution, halo masses are permitted to decrease with time if indicated by the N-body simulation, and subhaloes are permitted to jump between branches of merger trees (and between separate merger trees) if indicated.

Halo finder properties used The standard incarnation of GALACTICUS uses $M_{\rm bnd}$ but runs have been performed for all of the five supplied mass definitions. GALACTICUS further uses the following information from the provided halo catalogues: haloid, hosthaloid, number of particles, mass, radius, concentration, spin parameter, angular momentum, position, and velocity; if any of these values is not supplied (e.g. spin parameter), a random value is drawn from a distribution as measured by cosmological simulations. Further, the peak value of the circular velocity curve and the velocity dispersion are carried through the code, but not used for any calculation.

A2 GALICS-2.0 (Cattaneo, Blaizot, Devriendt & Mamon)

GALICS-2.0 is not a simple development of GALICS (Hatton et al. 2003; Cattaneo et al. 2006), but a totally new and different code. Its main characteristics are presented here for the first time and hence described in more detail for than the other models.

Gas accretion A baryonic mass $M_{\rm b} = f_{\rm b} M_{\rm h}$ is assigned to a halo of mass $M_{\rm h}$. Let $T_{\rm reio}$ be the temperature at which the intergalactic medium is reionised; $f_{\rm b} = f_{\rm b}(M_{\rm h}, z)$ is a function such that $f_{\rm b} \sim 0$ at $T_{\rm vir} \ll T_{\rm reio}$ and $f_{\rm b} \sim \Omega_{\rm b}/\Omega_{\rm M}$ at $T_{\rm vir} \gg T_{\rm reio}$. Its precise form is irrelevant for this article because the N-body simulation used for this comparison has such poor resolution that it can resolve only haloes with $T_{\rm vir} \gg T_{\rm reio}$. The baryonic mass that accretes onto a halo between two timesteps is the maximum between $\Delta M_{\rm b}$ and zero. A fraction $f_{\rm hot} = f_{\rm hot}(M_{\rm h}, z)$ of this gas is shock heated and added to the hot halo. The rest is put into cold streams, which accrete onto the disk of the central galaxy on a dynamical timescale. Cosmological hydrodynamic simulations show that $f_{\rm hot} \sim 0$ at $M_{\rm h} \lesssim 3 \times 10^{10}\, M_\odot$ and that $f_{\rm hot} \sim 1$ at $M_{\rm h} > 3 \times 10^{12}\, M_\odot$ (Ocvirk et al. 2008; Nelson et al. 2013). The halo mass M_h at which $f_{\rm hot} = 0.5$ increases with redshift (at least at $z > 2$). In this paper, we assume that f_h is a linear ramp between the halo mass $M_{\rm shock\,min}$ at which some gas begins to be shock heated and the halo mass $M_{\rm shock\,max}$ above which the infalling gas is entirely shock heated. We assume that $M_{\rm shock\,max} = M_{\rm shock} + \alpha(z - z_{\rm c})$ for $z > z_{\rm c}$ and that $M_{\rm shock\,max} = M_{\rm shock}$ for $z \leqslant z_{\rm c}$ where $z_{\rm c}$, $M_{\rm shock}$ and $M_{\rm shock\,min}$ are free parameters of the model to be

determined by fitting observational data. On a theoretical ground, $M_{\rm shock}$ is the critical mass halo mass at which the cooling time equals the gravitational compression time and $z_{\rm c}$ is the critical redshift at which $M_{\rm shock}$ equals the non-linear mass (Dekel & Birnboim 2006).

Cooling Following Cattaneo et al. (2006) and Dekel et al. (2009), we assume that galaxies are built through the accretion of cold gas and that hot gas never cools. This is an extreme assumption, but is in good agreement with the galaxy colour-magnitude distribution, while, if we let the gas cool, the predictions of the model are in complete disagreement with the observations (Cattaneo et al. 2006). Introducing cooling makes sense only if one has a physical model of how AGN feedback suppresses it. Attempts in this direction have been made, starting from (Croton et al. 2006), but the physics are uncertain. Hence it was considered that not much would be gained from implementing them in GALICS-2.0.

Star formation Following (Bigiel et al. 2008), we assume a constant star formation timescale of $t_{\star\,\rm d} = 2.5 \times 10^9\,{\rm yr}$ for disks and $t_{\star\rm b} = 2.5 \times 10^8\,{\rm yr}$ for bulges (merger-driven starbursts) for all gas. $\dot{M}_\star = M_{\rm gas}/t_\star$, where $M_{\rm gas}$ is the gas mass in the component. Star formation is suppressed when $\Sigma_{\rm gas} < 1\,{\rm M}_\odot\,{\rm pc}^{-2}$. Disks with $\Sigma_{\rm gas} > 20\,{\rm M}_\odot\,{\rm pc}^{-2}$ are assumed to be in a starburst mode and are assigned the same star formation timescale as bulges. Not only are these assumptions observationally motivated, but also they have the practical advantage that star formation rates are affected only mildly by errors in the modelling of disk sizes.

Initial mass function As in Cattaneo et al. (2006), we assume a Kennicutt (1983) stellar initial mass function. The IMF that our model uses is determined by our choice of input stellar evolution tables (see Metal treatment below).

Metal treatment Stars are created with metallicity that equals that of the gas from which they form. Stellar evolution is computed following Pipino et al. (2009), who tabulated the mass loss rate and the metal yield of a stellar population as a function of its age and metallicity. We can select different stellar evolution models/IMFs by replacing the input file with the stellar evolution tables.

Supernova feedback and winds Matter ejected from stars is mixed into the interstellar medium. The mass outflow rate through stellar feedback is assumed to be given by $\dot{M}_{\rm w} = (M_{\rm h}/M_{\rm SN})^\beta \dot{M}_\star$, where $\dot{M}\star$ is the star formation rate, while $M_{\rm SN}$ (the halo mass at which outflow rate equals star formation rate) and $\beta < 0$ are free parameters of the model. We consider a scaling with M_h rather than with $v_{\rm c}$ because the latter would lead to weaker feedback at high redshift for a same halo mass.

Gas ejection & reincorporation As our model does not include cooling, it is irrelevant whether the gas that is blown out of the galaxy escapes from the halo or whether it is mixed to the hot component, as we assume currently.

Disk structure Gas that accretes onto a galaxy contributes to the disk's angular momentum $\mathbf{J}_d$ with specific angular momentum that equals that of the halo at the time of accretion. The disk radius r_d is computed by assuming that the disk is exponential and by solving the equation

$$|\mathbf{J}_d| = \frac{M_d}{r_{\rm d}^2} \int_0^\infty {\rm e}^{-\frac{r}{r_{\rm d}}} [v_{\rm d}^2(r) + v_{\rm b}^2(r) + v_{\rm h}^2(r)]^{\frac{1}{2}} r^2\,{\rm d}r, \quad \text{(A1)}$$

where the disk term $v_{\rm d}$, the bulge term $v_{\rm b}$, and the halo term $v_{\rm h}$ are the three terms that contribute in quadrature to disk's rotation curve. The halo term v_h is computed by assuming that the halo follows an NFW profile modified by adiabatic contraction (Blumenthal et al. 1986).

Disk instability Disk instabilities are not enabled yet because we first want the test the properties of disks and bulges in a scenario in which mergers are the only mechanism for the formation of bulges.

Starburst Gas is starbursting after a major merger or when $\Sigma_{\rm gas} > 100\,M_\odot\,{\rm pc}^{-2}$. In these cases, we lower the star formation timescale from $t_{\star\,\rm d} = 2.5 \times 10^9\,{\rm yr}$ to $t_{\star\rm b} = 2.5 \times 10^8\,{\rm yr}$.

AGN feedback Two types of AGN feedback have been suggested in the literature: one is related powerful AGN, the other is mainly linked to Fanaroff-Riley type I radio sources. The need for the former is unclear while the second is essential to explain the absence of cooling flows in massive systems (Cattaneo et al. 2009). Our code does not contain any explicit model of AGN feedback. However, the assumption that the hot gas never cools is an implicit model for AGN feedback. It corresponds to the assumption that $P_{\rm jet} = L_{\rm X}$, i.e., that that jets self-regulate so that the power they damp into the hot gas matches exactly that which is lost to X-rays (see, e.g., Cattaneo & Teyssier 2007). Observationally, these quantities are equal to $\sim 10\%$ (Cattaneo et al. 2009, and references therein). Hence, this is a reasonable first approximation.

Merger treatment In minor mergers (mass ratio $< 1:3$), the disk and the bulge of the smaller galaxy are added to the disk and the bulge of the larger galaxy, respectively. In major mergers, the galaxies are scrambled into one large bulge and a fraction $\epsilon_\bullet$ of their gas content feeds the growth of a central supermassive black hole (Cattaneo et al. 2009). The size of the merger remnant is computed by applying an energy conservation argument that has been tested in hydrodynamic simulations (Covington et al. 2011; Oser et al. 2012). Our calculation assumes that merging pairs start with zero energy of interaction at infinity in agreement with what we see in cosmological hydrodynamic simulations and with the constraints from the mass-size relation (Shankar et al. 2013, 2014).

Substructures Substructures are traced from the N-body simulation. No gas accretion is allowed onto them but cold gas already accreted keeps streaming onto satellite galaxies as long as the host halo mass is $M_h < M_{\rm shock\,max}$.

Orphans Whenever the code encounters a halo with more than one progenitor, it computes the dynamical friction time for all progenitors bar the most massive one. The dynamical friction time is computed with Jiang et al. (2008)'s formula as in Cattaneo et al. (2011). This formula is a modification of Chandrasekhar (1943)'s (see Binney & Tremaine 2008) that includes the effects of orbital eccentricity and that has been calibrated on the results of cosmological simulations. Our calculation of the dynamical friction time contains a fudge factor $\epsilon_{\rm df}$ that is a free parameter of the model. A halo/subhalo merges with its descendent according the merger tree only after this time has elapsed. The halo catalogues are completed with the creation of a ghost halo at all timesteps between the one

when the halo/subhalo was last detected and the elapsing of the dynamical friction time. If $\epsilon_{\rm df} = 0$, the dynamical friction time is set equal to zero. Hence halo/subhalo mergers result into immediate galaxy mergers.

Parameters and calibration method For this project, the code has been calibrated manually by requiring that it fits the evolution of the galaxy stellar mass function at $0 < z < 2.5$ (Baldry et al. 2012; Ilbert et al. 2013; Bernardi et al. 2013). The parameters that have been tuned and that are relevant for this comparison are:

- The mass $M_{\rm shock\,min}$ above which shock heating begins and the three parameters $M_{\rm shock}$, α and $z_{\rm c}$ that determine the critical mass above which shock heating is complete.
- The star formation timescales for disks ($t_{\star\,\rm d}$) and bulges (merger-driven starbusts; $t_{\star\,\rm d}$), and the gas surface density threshold for star formation $\Sigma_{\rm min}$.
- The mass $M_{\rm SN}$ at which outflows rate equal star formation rate and the exponent β of the scaling of mass-loading factor with halo mass.
- The dynamical friction parameter $\epsilon_{\rm df}$.
- The critical mass ratio μ that separates minor and major mergers.

Here we have used $M_{\rm shock\,min} = 10^{10.5}\,M_\odot$, $M_{\rm shock} = 10^{12.3}\,M_\odot$, $\alpha = 0.3$, $z_{\rm c} = 1.5$ and $M_{\rm SN} = 4 \times 10^{11}\,M_\odot$ (for $h = 0.678$). The best fit to the galaxy stellar mass function of Baldry et al. (2012) is found for $\beta = -2$ and $\epsilon_{\rm df} > 0$ (our best fit is for $\epsilon_{\rm df} \ll 1$; hence we apply Occam's razor and prefer a model with no ghost/orphans). The star formation timescales for disks ($t_{\star\,\rm d} = 2.5 \times 10^9\,$yr) and merger-driven starbursts ($t_{\star\,\rm d} = 2.5 \times 10^8\,$yr) and the gas surface density threshold for star formation $\Sigma_{\rm min} = 1\,M_\odot\,{\rm pc}^{-2}$ were not tuned but they were set to the values found observationally by Bigiel et al. (2008). The critical mass ratio of $\mu = 1/3$ that separates minor and major mergers was not tuned either.

Model origin The model was conceived to be run on merger trees from N-body simulations.

Modifications to the supplied data None besides the creation of ghost haloes if $\epsilon_{\rm df} > 0$.

Halo finder properties used They halo properties that enter the GALICS-2.0 SAM are the halo mass $M_{\rm halo}$, its radius $R_{\rm halo}$ and the halo angular momentum $\mathbf{J}_{\rm halo}$ (the virial velocity is computed with the formula $v_{\rm c}^2 = GM_{\rm halo}/R_{\rm halo}$). Positions and velocities are used to compute dynamical friction and tidal stripping. Halo concentration is needed to compute dynamical friction, tidal stripping, and the radii of disks and bulges, but it is not provided in the SUBFIND catalogues. Hence, it has been computed with the fitting formulae of Muñoz-Cuartas et al. (2011). GALICS-2.0 flags certain haloes as bad. Bad haloes have positive total energy or they are tidal features that broke off a good halo, in which case we assume that no galaxy is formed in them. Normally, there is no gas accretion onto haloes that are flagged as bad. We could not impose this condition here because halo kinetic and potential energies were not provided but this is unlikely to affect our results because the halo/subhalo finder SUBFIND automatically removes unbound particles.

A3 MORGANA (Monaco & Fontanot)

In this paper we use the version of MORGANA that has been presented in Lo Faro et al. (2009). Its main properties are detailed below.

Cooling Described in detail in Viola et al. (2008), the model assumes that the gas is in hydrostatic equilibrium within an NFW halo and polytropic. Its thermal state responds to the injection of energy. The cooling radius is treated as a dynamical variable. Disk sizes are computed using the Mo et al. (1998) model, taking into account the presence of a bulge.

Star formation Star formation is treated following the results of the model by Monaco (2004).

Initial mass function A Chabrier (2003) IMF is assumed.

Metal treatment An Instantaneous Recycling Approximation is assumed, only global metallicities are followed.

Supernova feedback and winds Feedback and winds are treated following the results of the model by Monaco (2004). The ejection rate of gas into the halo is always equal to the star formation rate.

Gas ejection & reincorporation The halo acts as a buffer for feedback. Galaxies inject (hot or cold) mass and (thermal or kinetic) energy in the halo, when the typical specific energy is larger than the escape velocity of the halo the gas is ejected into the IGM. Half of this ejected gas is re-accreted whenever the circular velocity of the halo grows larger than the velocity at ejection.

Disk instability The Efstathiou et al. (1982) criterion is used.

Starburst The size of star-forming gas in bulges is estimated by assuming that its velocity dispersion is determined by turbulence injected by SN feedback. SFR is computed using a Kennicutt law, the high gas surface densities guarantees short gas consumption timescales.

AGN feedback Star formation in the bulge is responsible for the loss of angular momentum of a fraction of gas; the reservoir of such low-angular momenum gas is accreted onto the BH on a viscous time-scale. The accretion is Eddington-limited. AGN feedback can be in the quasar mode or in the 'jet' (radio) mode if the accretion rate in units of the Eddington one is higher or lower than 0.01.

Merger treatment Major mergers transform the whole resulting galaxy into a bulge, a minor merging satellite is put in the galaxy bulge. A fraction of 80% of stars in minor merging satellites is positioned into the stellar halo component.

Substructures The N-body simulation subhalo information is not used to follow the orbital evolution of substructures; they are rather tracked analytically. In detail, whenever a DM halo merges with a larger structure, the orbital decay of its galaxies is computed using an updated version of the fitting formulae provided by Taffoni et al. (2003), calibrated on the results of numerical simulations, which account for dynamical friction, tidal stripping and tidal disruption.

Orphans All satellite galaxies are effectively treated as 'orphans', i.e. the subhalo information is not explicitly used in modeling their evolution.

Calibration method Parameters were manually to fit the stellar mass function of galaxies at $z = 0$ and the evolution of the SFR density; see Lo Faro et al. (2009) for more details.

Model origin MORGANA has been designed to work with the idealized merger trees obtained with the PINOCCHIO code (Monaco et al. 2002), so the application to numerical merger trees requires a significant amount of cleaning of the trees.

Modifications to the supplied data It is assumed that the merger trees of haloes are mirrored by the evolution of their main haloes, so that main haloes either have no progenitors or have at least one main halo progenitor. When this is not true, the merger tree is modified to adapt to this requirement. This includes the reabsorption of any substructure that descends into a main halo (a 'backsplash' halo) or the exchange of the role of main halo between two haloes.

Halo finder properties used As a halo mass, our adopted default choice is the FOF mass $M_{\rm fof}$, but we run the model on all five mass definitions. However, the halo mass used to obtain the budget of baryons available to the halo is assumed never to decrease, so it is computed as the maximum of the total mass that the halo and all its progenitors have got in the past. In addition to this MORGANA made use of the provided haloid, hosthaloid, number of substructures, number of particles, position, and velocity.

A4 SAG (Cora, Vega-Martínez, Gargiulo & Padilla)

While the SAG model originates from a version of the Munich code (Springel et al. 2001b), it has seen substantial development and improvement; we are going to explain its features (and derivations from the Munich and other models) here.

Cooling A gaseous disk with an exponential density profile is formed from gas inflow generated as the result of the radiative gas cooling suffered by the hot gas in the halo (Springel et al. 2001). The metal-dependent cooling function is estimated by considering the radiated power per chemical element given by Foster et al. (2012) multiplied by the chemical abundances of each element in the hot gas, thus being completely consistent with the metallicity of this baryonic component.

Star formation When the mass of the disk cold gas exceeds a critical limit, an event of quiescent star formation takes place, as in Croton et al. (2006).

Initial mass function SAG assumes a Salpeter IMF.

Metal treatment SAG includes a detailed chemical implementation (Cora 2006), which estimates the amount of metals contributed by stars in different mass ranges. Metals are recycled back to the cold gas taking into account stellar lifetimes (Padovani & Matteucci 1993). The code considers yields from low- and intermediate-mass stars (Karakas 2010), mass loss of pre-supernova stars (Hirschi et al. 2005), and core collapse supernovae (SNe CC, Kobayashi et al. 2006). Ejecta from supernovae type Ia (SNe Ia) are also included (Iwamoto et al. 1999); SNe Ia rates are estimated using the single degenerate model (Lia et al. 2002).

Supernova feedback and winds Feedback from SNe CC is modeled following De Lucia et al. (2004a). The amount of reheated gas is proportional to the energy released by SNe CC and inversely proportional to the square of the halo virial velocity. Cora (2006) adapted this prescription according to the chemical model implemented, such that the energy contribution of SNe CC occurs at the moment of their explosions, for which the lifetimes of massive stars are considered. SNe feedback produces outflows of material that transfer the reheated cold gas with its metal content to the hot gas phase; this chemical enrichment has a strong influence on the amount of hot gas that can cool, since the cooling rate depends on the hot gas metallicity.

Gas ejection & reincorporation SAG assumes a 'retention' scheme in which the cold gas reheated by SNe feedback is transfered to the hot gas phase, being available for further gas cooling that takes place only in central galaxies ('strangulation' scheme).

Disk instability When a galactic disk is sufficiently massive that its self-gravity is dominant, it becomes unstable to small perturbations by satellite galaxies. The circular velocity of the disk involved in the stability criterion of Cole et al. (2000) is approximated by the velocity calculated at three times the disk scale-length, where the rotation curve flattens (see Tecce et al. 2010, for details concerning disk features). We model the influence of a perturber by computing the mean separation between galaxies in a group; the instability is triggered when this separation is smaller than a certain factor (a free parameter of the model) of the disk scale radius of the perturbed galaxy. When an unstable disk is perturbed, existing stars are transferred to the bulge component along with the cold gas that is consumed in a starburst.

Starburst Starbursts occur in both mergers and triggered disk instabilities and are the only channel for bulge formation. During a starburst episode, we consider that the cold gas available in the bulge that has been transfered from the disk, referred to as bulge cold gas, is gradually consumed. The period for star formation is chosen to be the dynamical time-scale of the disk. However, as the starburst progresses, effects of supernovae feedback, recycling of gas from dying stars and black hole growth modify the reservoir of cold gas of both disk and bulge, thus also changing the time-scale of the starburst (Gargiulo et al. 2014).

AGN feedback SAG includes radio-mode AGN feedback following Croton et al. (2006) as described in Lagos et al. (2008), which reduces the amount of gas that can cool thus providing a mechanism for regulating star formation in massive galaxies. AGNs are produced from the growth of central black holes, for which two possible mechanisms are considered: i) infall of gas towards the galactic centre, induced by merger events or disk instabilities, and ii) the accretion of gas during the cooling process. The current version of the code (Gargiulo et al. 2014) considers that mass accretion rates in the latter case depends on the square of the virial velocity (being consistent with a Bondi-type accretion, Bondi 1952), instead of on the cube of the velocity as in Lagos et al. (2008), in order to prevent super massive black holes at the centre of cluster-dominant galaxies to grow unrealistically large, at the expense of the intracluster medium.

Merger treatment The galaxy inhabiting the subhalo is assumed to merge with the central galaxy of their host subhalo on a dynamical friction time-scale (Binney & Tremaine 1987). The merger can

be major or minor depending on the the baryonic mass ratio between the satellite galaxy and the central galaxy. If this mass ratio is larger than 0.3, then the merger is considered a major one. In this case, stars and cold gas in the disk of the remnant galaxy are transferred to the bulge, with the latter being consumed in a starburst. The presence of a starburst in a minor merger will depend on the fraction of cold gas present in the disk of the central galaxy, as implemented by Lagos et al. (2008). In minor mergers, only the stars of the merging satellite are transferred to the bulge component of the central galaxy.

Substructures Substructures are followed from the N-body simulation. The supplied data has not been modified. Those branches of merger trees that start with subhaloes give place to spurious galaxies with neither cold gas nor stars since gas cooling does not take place in galaxies residing in subhaloes. Those merger trees are ignored and we discard those galaxies in the output of SAG.

Orphans Orphan galaxies are created when their subhaloes are no longer identified after merging with a larger one because they lose mass as a result of tides. The position and velocity of orphan galaxies are estimated assuming a circular orbit with a velocity given by the virial velocity of the parent subhalo and a decaying radial distance determined by dynamical friction (Binney & Tremaine 1987).

Calibration method Calibrations of SAG are performed using the 'Particle Swarm Optimization' technique, which yields best-fitting values for the free parameters of the model allowing it to achieve good agreement with specific observational data (Ruiz et al. 2015). The free parameters that have been tuned are those related with star formation efficiency, the SNe feedback efficiencies that control the amount of disk cold gas and bulge cold gas reheated by the energy generated by SNe formed in the disk and in the bulge, respectively, parameters involved in the AGN feedback, that is, the fraction of cold gas accreted onto the central supermassive black hole (SMBH) and the efficiency of accretion of hot gas onto the SMBH, and finally, the factor involved in the distance scale of perturbation to trigger disk instability.

We calibrate the free parameters of the SAG model considering a set of observational constraints that involve the $z = 0$ luminosity function in the *r*-band (*r*-band LF), the relation between the mass of the central SMBH and the bulge mass (BHB relation), the redshift evolution of SNe Ia and SN CC rates, and the $[\alpha/\mathrm{Fe}]$-stellar mass relation of elliptical galaxies. The first two constraints help to tune the free parameters associated to the star formation efficiency and the SNe and AGN feedback. The third one allows to fix the fraction of binary stars that explode as SNe Ia, and therefore, the amount of iron recycled into the interstellar medium. The last one establishes more restriction to the efficiency of SNe feedback arising from stars formed in the bulge. The observational data used are the *r*-band LF of Blanton et al. (2005a), the BHB relation given by Häring & Rix (2004) and Sani et al. (2010), the compilation of rates for both SNe Ia and SNe CC given by Melinder et al. (2012), and the $[\alpha/\mathrm{Fe}]$ ratio of elliptical galaxies presented in Thomas et al. (2010) and Arrigoni et al. (2010).

Model origin While the SAG model originates from a version of the Munich code (Springel et al. 2001), based on N-body simulations, it has seen substantial development and has been improved with a detailed chemical implementation (Cora 2006), the inclusion of AGN feedback and disk instabilities (Lagos et al. 2008), a detailed estimation of disk scale-lengths Tecce et al. (2010), and a gradual star formation during starbursts (Gargiulo et al. 2014), among other aspects that are not taken into account in the version used for the current comparison, like the effects of accretion with misaligned angular momenta on the properties of galactic disks (Padilla et al. 2014), a star formation dependent top-heavy integrated galactic IMF (Gargiulo et al. 2014), estimation of nebular emission of star-forming galaxies (Orsi et al. 2014), and environmental effects such as tidal stripping and ram pressure stripping (Cora et al., in prep.).

Modifications to the supplied data As mentioned above, branches of the merger tree that start with subhaloes are ignored. However, they contribute to generate the galaxy population if gradual removal of hot gas is allowed since, in that case, satellites receive cooling flows (which, however, is not the case in the version of the model considered here). No other modifications have been made.

Halo finder properties used SAG uses the bound mass M_{bnd} to construct its galaxies. Further properties entering SAG are the haloid, hosthaloid, number of substructures, radius, position, velocity, and spin parameter.

A5 SANTACRUZ (Somerville & Hirschmann)

The SANTACRUZ SAM was first presented in Somerville & Primack (1999) and significantly updated in Somerville et al. (S08 2008), Somerville et al. (2012), Hirschmann et al. (2012, H12), and recently in Porter et al. (2014, P14). The SANTACRUZ SAM includes the following physical processes: (1) shock heating and radiative cooling of gas, (2) conversion of cold gas into stars via an empirical 'Kennicutt-Schmidt' relation, (3) starbursts, black hole feeding, and morphological transformation due to galaxy mergers 4) bulge and black hole growth via 'disk instabilities' 5) metal enrichment of the interstellar and intracluster media by supernovae using the instantaneous recycling approximation 6) galactic outflows driven by stars and supernovae (7) galactic outflows driven by 'quasar mode' black hole activity, and heating of the hot intracluster and intragroup medium by 'radio mode' black hole activity. The code used here adopts the modifications relative to the S08 model suggested by Hirschmann et al. (2012) in order to match the observed luminosity function of AGN: massive seed black holes, black hole feeding via disk instabilities, and suppressed black hole feeding in mergers at low redshift (see H12 for details). These modifications have almost no impact on galaxy properties but do affect black hole growth.

Cooling The cooling model is based on the spherically symmetric cooling flow model originally presented in White & Frenk (1991), and is described in detail in S08 and P14. We assume a singular isothermal profile for the hot gas density distribution and adopt the metallicity dependent cooling functions of Sutherland & Dopita (1993). If the cooling radius is larger than the virial radius, gas is accreted on a halo dynamical time. Cooling gas is only accreted onto 'central' galaxies.

Star formation As gas cools, we assume that it settles into a rotationally-supported exponential disk. We use a prescription based on the work of Mo et al. (1998) and Somerville et al. (2008) to compute the radial size of the gas disk.

We allow for two modes of star formation: 'disk mode' star formation, which occurs in disks at all times as long as cold gas

above a critical surface density is present, and 'burst mode' star formation, which occurs after two galaxies merge. In the 'disk mode' the star formation rate density is dependent on the surface density of cold gas in the disk, following the empirical Schmidt-Kennicutt relation (Kennicutt 1998). Only gas that is above a critical surface density threshold is allowed to form stars. See S08 and P14 for further details.

Initial mass function We adopt a Chabrier (2003) initial mass function.

Metal treatment We model chemical enrichment using the instantaneous recycling approximation. The chemical yield is treated as a free parameter.

Supernova feedback and winds Massive stars and supernovae are assumed to produce winds that drive cold gas back into the ICM and IGM, heating the gas in the process. The mass outflow rate is proportional to the star formation rate,

$$\dot{m}_{\rm rh} = \epsilon_{\rm SN} \left(\frac{200 \text{ km s}^{-1}}{V_{\rm disk}} \right)^{\alpha_{\rm rh}} \dot{m}_*, \qquad \text{(A2)}$$

where $\epsilon_{\rm SN}$ and α_{rh} are free parameters and $V_{\rm disk}$ is the circular velocity of the disk.

Gas ejection & reincorporation The proportion of the gas that is ejected from the halo entirely is a decreasing function of the halo's virial velocity. This gas can then fall back into the hot halo, at a re-infall rate that is proportional to the mass of the ejected gas and inversely proportional to the dynamical time of the halo (see S08 and P14 for details). When gas is ejected due to supernova feedback, these winds are assumed to have a metallicity $Z_{\rm cold}$. Ejected metals are assumed to "re-infall" back into the hot halo on the same timescale as the gas.

Disk instability We include bulge formation and black hole growth due to disk instabilities as in the "stars" model of P14 (see also H12). Following Efstathiou et al. (1982) we define the stability parameter

$$\epsilon_{\rm disk} = \frac{V_{\rm max}}{(GM_{\rm disk}/r_{\rm disk})^{1/2}}, \qquad \text{(A3)}$$

where $V_{\rm max}$ is the maximum circular velocity of the halo, $r_{\rm disk}$ is the scale length of the disk, and $M_{\rm disk}$ is the mass of stars in the disk. Disks are deemed unstable if $\epsilon_{\rm disk} < \epsilon_{\rm crit}$, where $\epsilon_{\rm crit}$ is a free parameter. In every timestep in which the disk becomes unstable, we move just enough stars from the disk to the bulge component to restore stability.

Starburst Following a merger with mass ratio $\mu > \mu_{\rm crit} \sim 0.1$, we trigger a burst of star formation. The burst mode star formation is added onto the 'disk'-mode star formation described above. The efficiency and timescale of the burst mode depends on the merger mass ratio, the gas fraction of the progenitors, and the circular velocity of the progenitors, as described in S08. These scalings were derived from hydrodynamic simulations of binary galaxy-galaxy mergers (see S08 for details).

AGN feedback In addition to triggering starbursts, mergers drive gas into galactic nuclei, fueling black hole growth. Every galaxy is born with a small "seed" black hole (typically $\sim 10^4\,{\rm M}_\odot$ in our standard models). Following a merger, any pre-existing black holes are assumed to merge fairly quickly, and the resulting hole grows at its Eddington rate until the energy being deposited into the ISM in the central region of the galaxy is sufficient to significantly offset and eventually halt accretion via a pressure-driven outflow. This results in self-regulated accretion that leaves behind black holes that naturally obey the observed correlation between BH mass and spheroid mass or velocity dispersion (see S08 and H12 for more details). Large-scale winds associated with this rapid BH growth can also remove gas from the galaxy (see S08).

A second mode of black hole growth, termed "radio mode", is assumed to couple very efficiently with the hot halo gas, and to provide a heating term that can partially or completely offset cooling during the "hot flow" mode (we assume that the jets cannot couple efficiently to the cold, dense gas in the infall-limited or cold flow regime).

Merger treatment Once haloes cross the virial radius of a parent halo, the Santa Cruz SAM tracks the timescale for the orbits of the sub-haloes (satellites) to decay via dynamical friction using a refined version of the Chandrasekhar formula (see S08). Dark matter is stripped from the sub-haloes on each orbit. If the sub-halo is stripped below a critical mass, it and the galaxy it contains are considered to be tidally disrupted and the stars in the galaxy are added to the 'diffuse stellar halo'. Any cold gas is considered to be heated and added to the hot gas halo of the host. Galaxies that are not tidally destroyed before they reach the center are merged with the central galaxy. Following a merger, a fraction $f_{\rm scat}$ of the stars from the satellite are added to the diffuse interstellar halo. Depending on the merger mass ratio and the gas fraction of the progenitors, some of the disk stars are moved to the bulge following a merger (see P14).

Substructures Sub-structures are tracked analytically. One minor issue is that our SAM cannot track haloes that become sub-haloes and then travel outside the virial radius of the host (so-called 'backsplash galaxies', e.g. Gill et al. 2005)– we continue to treat these as sub-haloes.

Orphans All substructures are effectively treated as 'orphans' in our models.

Calibration method The SAM parameters used here are identical to those used in Porter et al. (2014). These parameters were chosen by tuning to observations of the galaxy stellar mass function, gas fraction and stellar metallicity as a function of stellar mass, and black hole mass versus bulge mass relationship, all at $z \sim 0$ (see S08 and P14 for details). In addition, our "disk instability" parameter is tuned to attempt to reproduce the morphological mix of nearby galaxies as a function of stellar mass (see P14).

Model origin The SANTACRUZ SAM was originally developed based on EPS merger trees (Somerville & Primack 1999). Subsequently, the model has been implemented within merger trees extracted from the Bolshoi simulations (P14). Our model results are quite insensitive to whether we use EPS mergers trees or high-quality N-body merger trees.

Modifications to the supplied data Currently the SANTACRUZ SAM does not make use of positional information from the N-body simulation for "sub-haloes", haloes that have become subsumed in other virialized haloes. As a result sub-haloes were stripped from

the merger trees provided for this project. No further modifications were made.

Halo finder properties used The SANTACRUZ SAM uses the $M_{\rm BN98}$ 'virial mass' definition by default. The only halo finder properties that we use are the halo mass and redshift, and progenitor and descendant relationships.

A6 YSAM (Lee & Yi)

Here we briefly summarize the main features of YSAM. It has been developed to calculate galaxy properties on halo merger trees extracted from N-body simulations. YSAM assumes that haloes newly identified in a volume have hot gas components proportional to their virial mass, following the universal baryonic fraction, $\Omega_{\rm b}/\Omega_{\rm m}$. The hot gas components are cooled (see below). Cold gas components form gas disks and stellar populations are newly born in the disks by the simple law in Kauffmann et al. (1993). Gradual mass loss from stellar populations can enrich the metallicity of galaxies by recycling the ejecta in hot and cold gas reservoirs. YSAM also includes feedback processes (see below). In addition, environmental issues can affect the gas components of subhaloes: hot gas is stripped by tidal forces (see Kimm et al. 2011) and ram pressure (McCarthy et al. 2008; Font et al. 2008). Perhaps the most notable difference of YSAM is that it calculates stellar mass loss in all constituent stellar populations in each galaxy step by step. This often involves tracking tens of thousands of separate populations in each galaxy, which helps to trace the gas recycling more realistically than in the case of instant recycling assumption. Further details can be found in Lee & Yi (2013).

Cooling YSAM calculates gas cooling rates by adopting the prescription proposed by White & Frenk (1991).

Star formation YSAM follows a simple law suggested by Kauffmann et al. (1993) for quiescent star formation.

Initial mass function Chabrier, Salpeter, and Scalo IMFs are available in ySAM. Stellar populations formed in quiescent and bursty modes can have different IMFs.

Metal treatment YSAM calculates stellar mass loss from every single stellar population at each time step. The amount of metals in the ejecta is computed based on a given IMF and chemical yields of Type Ia (Nomoto et al. 1984) and Type II SNe (Portinari et al. 1998), and intermediate mass stars (Marigo 2001). The metals can be recycled by star formation or circulated between galaxies and environments via gas cooling or heating.

Supernova feedback and winds YSAM follows the prescriptions described in Somerville et al. (2008) for SN feedback and winds.

Gas ejection & reincorporation Gas components can be blown away by SN and QSO mode AGN feedback. Some of them can be re-accreted onto galaxies in the dynamical timescale of haloes.

Disk instability In YSAM, disk instability can be estimated by using a formula derived by Efstathiou et al. (1982). Due to uncertainties of disk instability (e.g. Athanassoula 2007), however, we turn it off in this study.

Starburst The amount of stars born in bursty mode is evaluated when galaxy mergers ($M_2/M_1 > 0.1$) take place. It is calculated following the prescriptions formulated by Somerville et al. (2008) from the numerical simulations performed by Cox et al. (2008).

AGN feedback QSO and radio modes AGN feedback has been implemented into YSAM by following Croton et al. (2006).

Merger treatment Satellite galaxies merge into their centrals when subhaloes harbouring them reach very central region of host haloes ($< 0.1R_{\rm vir}$). If a subhalo is deprived of mass below baryonic mass, then the galaxy at the centre of the subhalo is considered to be disrupted and their stellar components become diffuse stellar components of its host halo.

Substructures YSAM traces substructures following the results from the N-body simulation.

Orphans If a substructure disappears before reaching the central region of its host halo, YSAM calculates its mass (Battin 1987) and orbit (Binney & Tremaine 2008) analytically until approaching the very central regions. This has a large impact on the lifetime of subhaloes and galaxy merging timescale (Yi et al. 2013).

Calibration method YSAM has been manually calibrated to match galaxy mass functions (mainly that in Panter et al. 2008), BH-bulge relation (Häring & Rix 2004), global star formation density evolution (Panter et al. 2008), and stellar-to-halo mass relation (Moster et al. 2010).

Model origin YSAM has been developed to be run based on halo merger trees extracted from N-body simulations.

Modifications to the supplied data We ignore halo merger trees that disappear as independent host haloes before merging into other haloes. We also remove merger trees identified as subhaloes at the beginning. If, however, haloes born as subhaloes come out of their hosts and remain as host haloes by $z = 0$, then we do not discard them.

Halo finder properties used YSAM adopts as its prime mass $M_{\rm 200c}$ and also uses the following information from the supplied halo catalogues: haloid, hosthaloid, radius, position, and velocity; the number of particles, peak value and position of the circular rotation curve, and spin parameter are also read, but not used.

A7 Durham - GALFORM (Gonzalez-Perez, Bower & Font)

GALFORM-GP14, GALFORM-KB06 & GALFORM-KF08

For the study presented here we use the Gonzalez-Perez et al. (2014) (thereafter GALFORM-GP14) flavour of the GALFORM model (Cole et al. 2000), which exploits a Millenium Simulation-class N-body run performed with WMAP7 cosmology. We also compare the results from two variations of the GALFORM-GP14 model, to which we refer to as GALFORM-KB06 and GALFORM-KF08. These have been generated by running a modified version of the GALFORM-GP14 that accounts for the main differences with respect to the Bower et al. (2006) and Font et al. (2008) models. These two models were developed using merger trees derived from the Millennium simulation (Springel et al. 2005), which assumes a cosmology close to that from WMAP1.

The model referred here as GALFORM-KB06 is the GALFORM-GP14 model run assuming a single star formation law. The model referred here as GALFORM-KF08 is the GALFORM-GP14 model run assuming a single star formation law and including a gradual stripping of hot gas in satellite galaxies as opposed to the strangulation assumed by default.

Cooling Cooling rates are estimated by defining a cooling radius, assuming that the shock-heated halo gas is in collisional ionization equilibrium. The gas density profile in the halo is kept fixed and is well fit by the β-model (Cavaliere & Fusco-Femiano 1976) generally used to model hot X-ray emitting gas in galaxy clusters. We use the cooling functions tabulated by Sutherland & Dopita (1993), which are a function of both the metallicity and temperature of the gas.

Star formation The GALFORM-GP14 model assumes two different star formation laws depending on the star formation being quiescent, happening in disks, or happening in a burst. In the star burst mode, the star formation rate is assumed to be simply proportional to the mass of cold gas present in the galaxy and inversely proportional to star formation time-scale. This is what is also assumed for the quiescent star formation in both the GALFORM-KB06 and GALFORM-KF08 model variants. The quiescent star formation in the GALFORM-GP14 model is obtained in a self consistent calculation in which HI and H_2 are tracked explicitly and the star formation in disks is assumed to depend on the amount of molecular gas, H_2, rather than on the total mass of cold gas (Lagos et al. 2011).

IMF A Kennicutt IMF is assumed.

Metal treatment The model uses the instantaneous recycling approximation, with a recycled fraction of 0.44 and a metal yield of 0.021.

Supernova feedback and winds The supernova feedback efficiency is quantified in the model in terms of the rate at which cold gas is reheated and thus ejected into the halo, $\dot{M}_{\rm reheated}$, per unit mass of stars formed, ψ, which are computed as $\dot{M}_{\rm reheated} = \psi\left(\frac{v_{\rm circ}}{425\,{\rm km/s}}\right)^{-3.2}$.

Gas ejection & reincorporation The gas affected by stellar feedback is assumed to be heated to the virial temperature of the current halo and placed into a reservoir. The mass in this reservoir, $M_{\rm res}$, will return to the hot halo at a rate given by $1.26 \times M_{\rm res}/t_{\rm dyn}$, where $t_{\rm dyn}$ is the dynamical time-scale of the halo. The gas that has been reincorporated into the halo can then cool back on to the galaxy disk.

Disk instability If a disk is strongly self-gravitating it will be unstable with respect to the formation of a bar. This will happen in those disks satisfying the Efstathiou et al. (1982) criterion, with a stability threshold of 0.8.

Starburst During star bursts episodes, the star formation law assumed in the GALFORM-GP14 model is different from the quiescent case (not so for the other two model variants). The available cold gas is assumed to be consumed during a starburst event with a finite duration.

AGN feedback The onset of the AGN supression of the cooling flow can only happen in the model in haloes undergoing quasi-hydrostatic cooling. This is assumed to happen for haloes hosting galaxies such that $t_{\rm cool} > t_{\rm ff}/0.6$, where t_{cool} is the cooling time of the gas and t_{ff} is the free-fall time for the gas to reach the centre of the halo.

Merger treatment Mergers such that the ratio between masses exceeds 0.1 will trigger a burst of star formation. Disks are transformed into spheroids when mergers happen.

Substructures The N-body simulation subhalo information is used to trace substructure.

Orphans When the subhalo hosting a satellite galaxy can no longer be followed with the N-body simulation information, the Lacey & Cole (1993) analytical expression is used to compute the merging timescale of this orphan galaxy.

Calibration method The free parameters in this model where chosen manually such that the predicted luminosity functions in both b_J and K-band at redshift 0 and the predicted evolution of the rest-frame UV and V-band luminosity function were in reasonable agreement with observations (Norberg et al. 2002; Kochanek et al. 2001; Driver et al. 2012).

Model origin The GALFORM-GP14 model uses dark matter halo trees derived from the MS-W7 N-body simulation (Guo et al. 2013), with a simulation box of 500 Mpc/h side.

Modifications to the supplied data In order to run GALFORM, we have remapped the given merger trees using D-HALOES (Jiang et al. 2014). This algorithm groups subhaloes in N-body cosmological simulations avoiding transient structures and losses in mass. From the provided list of subhaloes, there is a percentage smaller than 15 per cent that D-HALOES classifies as independent haloes. This happens for haloes that when becoming subhaloes either retain more than 75 per cent their mass or that are located away from the main halo more than two half mass radii.

Halo finder properties used The standard GALFORM models use $M_{\rm bnd}$, but runs have been performed for all the five supplied mass definitions.

A8 Munich - DLB07 (De Lucia & Blaizot)

The variant of the Munich model described in De Lucia & Blaizot (2007b), with its generalization to the 3-yr Wilkinson Microwave Anisotropy Probe (WMAP3) cosmology discussed in Wang et al. (2008). The model includes prescriptions for gas cooling, star formation, stellar feedback, merger driven starburst, AGN feedback and chemical enrichment. The latter is based on an instantaneous recycling approximation. For more details on the physical models, we refer to Croton et al. (2006), De Lucia & Blaizot (2007b), and references therein.

Cooling The rate of gas cooling is computed following the model originally proposed by White & Frenk (1991), and an implementation similar to that adopted in Springel et al. (2001a). Full details can be found in De Lucia et al. (2010).

Star formation A Kennicutt-type prescription is adopted. Only gas above a critical surface density for star formation can be converted into stars. Details in Croton et al. (2006).

Initial mass function A Chabrier (2003) IMF is used throughout.

Metal treatment As detailed in De Lucia et al. (2004a), an instantaneous recycling approximation is adopted. Metals are ejected (and instantaneously mixed) into the cold gas component after each star formation event.

Supernova feedback and winds Supernovae explosions are assumed to reheat a (cold) gas mass that is proportional to the mass of stars formed. The amount of gas that leaves the dark matter halo in a wind is determined by computing whether the excess supernova energy is available to drive the flow after reheating the material to the halo virial temperature. Details can be found in Croton et al. (2006).

Gas ejection & reincorporation Ejected gas is re-incorporated into the hot gas component on a time-scale that is related to the dynamical time-scale of the halo, as detailed in De Lucia et al. (2004a).

Disk instability The instability criterion adopted is that of Efstathiou et al. (1982). When the instability condition is verified, we transfer enough stellar mass from the disk to the bulge so as to restore stability. For details, see again Croton et al. (2006) and De Lucia et al. (2011).

Starburst Galaxy mergers are accompained by starbursts modelled using the 'collisional starburst' prescription introduced by Somerville et al. (2001) with updated numerical parameters so as to fit the numerical results by Cox et al. (2004).

AGN feedback The model includes a distinction between a 'quasar mode' and a 'radio mode'. AGN feedback is implemented as detailed in Croton et al. (2006).

Merger treatment The model explicitly follows dark matter substructures. This allows us to follow properly the motion of the galaxies at their centres, until tidal truncation and stripping disrupt the subhalo at the resolution limit of the simulation. When this happens, a residual merger time is estimated using the current orbit and the classical dynamical friction formula of Binney & Tremaine (1987). For details, see De Lucia & Blaizot (2007b) and De Lucia et al. (2010).

Substructures The model follows dark matter haloes after they are accreted onto a larger system, i.e. substructures are explicitly followed from the N-body simulation.

Orphans An 'orphan' galaxy is created each time a substructure falls below the resolution limit of the simulation. The stellar mass of the galaxy is unaffected. The galaxy is assigned a residual merger time as detailed above. Its position and velocity are traced by following the most bound particle of the substructure at the last time it was present. As this information could not be reconstructed for this project positions and velocities of orphan galaxies are kept fixed to those of the substructures at the last time they were identified.

Calibration method The model has been calibrated 'by-hand' (note that in practice this means that a grid of model parameters was considered in order to evaluate the influence of each of them on model predictions). The main constrain is the K-band luminosity function at $z = 0$.

Model origin The model is designed to work with merger trees from N-body simulations.

Modifications to the supplied data No significant modification. Merger trees are reconstructed from original files provided, and using each halo's uniquely assigned descendant.

Halo finder properties used The following quantities from the supplied halo catalogue are used: snapnum, positions and velocities of each halo, its mass M_{200c} and spin parameter (this latter quantity is used to model the disk radius).

A9 Munich - LGALAXIES (Henriques, Srisawat & Thomas)

The 'Munich' model of galaxy formation is a semi-analytic scheme for simulating the evolution of the galaxy population as a whole and has been continually developed over the last quarter century (White & Frenk 1991; Kauffmann et al. 1993, 1999; Springel et al. 2001b, 2005). Recent updates to the baryonic physics have resulted in a model that is capable of reasonably describing the observed population of galaxies in the local Universe. These include a detailed treatment of gas reheating, ejection and reincorporation by supernova (De Lucia et al. 2004b), updated in Guo et al. (2011), black hole growth during mergers (Kauffmann & Haehnelt 2000) and feedback from quiescent accretion (Croton et al. 2006), continuous environmental effects acting on satellite galaxies (Guo et al. 2011), dust extinction from the ISM and molecular clouds (De Lucia & Blaizot 2007b). The model used in this paper, Henriques et al. (2013), includes all previous developments and aims at better representing the observed evolution of stellar mass across most of the age of the Universe. This is done by modifying the timescales for gas to be reincorporated after ejection from supernova in order to avoid an excessive build up of low mass galaxies at early times. As in Guo et al. (2013), a WMAP7 cosmology is adopted.

In the latest major release of the Munich model, (Henriques et al. 2014), the modifications implemented in Henriques et al. (2013) were combined with a less efficient ram-pressure striping implementation in low mass groups and a lower threshold for star formation. These ensure that low mass galaxies are predominately star forming down to $z = 0$ and that the model can simultaneously match the evolution of the stellar mass function and the fraction of red galaxies. In addition, the AGN feedback and dust model were adjusted in order to better follow the properties of intermediate and high-z galaxies, respectively. Although the Henriques et al. (2014) model provides a significantly better representation of the observable universe, we are unable to run it for this project since it requires information on the trajectories of most-bound particles for haloes striped below resolution. These are used to follow the dynamics of orphan galaxies and are crucially in order to track their properties. Without it, merger times and the disruption efficiency of satellites will be significantly different, changing the black-hole growth, star-burst efficiency and morphology evolution of all central galaxies. We therefore use Henriques et al. (2013) for which the combination of physics is less sensitive to these effects.

Cooling The cooling follows the implementation of White & Frenk (1991). Infalling diffuse gas is expected to shock-heat as it joins a halo. At early times and for low-mass haloes the post-shock cooling time is short and new material is assumed to settle onto the cold gas disk in a dynamical time. At later times and for higher mass haloes the shocked heated gas forms a quasi-static hot atmosphere from which it can gradually accrete to the centre via an element and temperature.

Star formation Following Kauffmann (1996), star formation is assumed to be proportional to the mass in cold gas above a given threshold.

Initial mass function A Chabrier (2003) IMF is assumed and 43% of the total mass of stars formed is assumed to be in massive, short lived stars, and immediately returned to the cold gas.

Metal treatment Following De Lucia et al. (2004a), these stars are enrich the surrounding medium with a fixed yield of metals. Fu et al. (2013) and Yates et al. (2013) implemented, respectively, more detailed models of star formation and chemical enrichment in the Munich model. This will be incorporated in future releases.

Supernova feedback and winds Supernova feedback is treated following De Lucia et al. (2004a) and Guo et al. (2011). The fraction of the total available energy used in feedback is parametrised in a virial velocity dependent way.

Gas ejection & reincorporation Part of the energy released during supernovae is used to reheat gas from the cold gas to the hot phase and the left-over used to eject material into an external reservoir. A new reincorporation model returns gas back into the hot phase at a rate inversely proportional to the halo mass (Henriques et al. 2013).

Disk instability Disk instabilities are followed as in Guo et al. (2011) and transport material inwards to the bulge and they occur in galaxies where self-gravity of the disk dominates the gravitational effects of the bulge and halo. When the instability criteria is met, we transfer sufficient stellar mass from the inner parts of the disk to the bulge to make it marginally stable again.

Starburst The stellar mass formed during a merger (see below) is modelled using the collisional starburst formulation of Somerville et al. (2001).

AGN feedback Henriques et al. (2013) includes two black-hole related processes: a "quasar" and a "radio" mode. Following Kauffmann & Haehnelt (2000), black holes are taken to form and grow when cold gas is driven to the centre of merging systems. Black holes are also allowed to accrete gas from the hot gas atmospheres of their galaxies. This is assumed to generate jets and bubbles which produce radio mode feedback, suppressing cooling onto the galaxy and so eliminating the supply of cold gas and quenching star formation (Croton et al. 2006).

Merger treatment When a satellite galaxy finally merges with the object at the centre of the main halo, the outcome is different for major and minor mergers. In a major merger, the disks of the two progenitors are destroyed and all their stars become part of of the bulge of the descendent, along with any stars formed during the merger. In a minor merger, the disk of the larger progenitor survives and accretes the cold gas component of the smaller galaxy, while its bulge accretes all the stars of the victim. Stars formed during the merger stay in the disk of the descendent.

Substructures When the host halo of a galaxy enters the virial radius of a larger system it becomes a satellite and its properties are strongly affected by a number of processes collectively called environmental effects. Satellite galaxies do not receive primordial infall, they are stripped of their hot and ejected gas components due to ram-pressure and tidal striping, and they might merge with other galaxies (Guo et al. 2011).

Orphans Once a satellite subhalo is disrupted, its central galaxy becomes an orphan and a merging clock is started. This will estimate how long the satellite will take to spiral into the central object due to dynamical friction. Since our implementation of tidal stripping of hot gas is directly connected to the stripping of dark matter, orphans have no hot or ejected gas. In addition, any cold gas reheated by supernovae is added to the central halo and tidal forces might completely strip the stars and cold gas into the intracluster medium.

In the default version of our model, the dynamical properties of orphan galaxies are given by those of the most bound particle identified at the time at which the halo falls below resolution. The vector offset is decayed due to dynamical friction. This has been shown to be crucial in order to correctly trace satellite distributions and achieve convergence for simulations of different resolution (Guo et al. 2011). Since the most bound particle information is not provided, the positions and velocities of orphans are frozen at the time of disruption and should be ignored. These do not have a significant impact on the physics in Henriques et al. (2013) which depend mostly on the independently calculated merger times but stop us from running the latest Henriques et al. (2014).

Calibration method The best-fit model was chosen by fully sampling the allowed regions in parameter space using the MCMC methodology described in Henriques et al. (2009, 2013). The stellar mass, K-band and B-band Luminosity functions at $z = 0, 1, 2$ and 3 were used as observational constraints.

Model origin Henriques et al. (2013) is built on N-body merger trees following the method introduced by Springel et al. (2001a). The substructure are followed directly from the dark-matter simulation and the supplied data was used in unmodified form. The following quantities from the supplied halo catalogue are used: snapnum, positions and velocities of each halo, its mass (M_{200c}200) and spin.

Modifications to the supplied data The supplied data was used in unmodified form. We note that insufficient information was supplied to allow use of the latest version of L-Galaxies (Henriques et al. 2014) which better models the stripping of satellite galaxies within groups and clusters.

Halo finder properties used The following quantities from the supplied halo catalogue are used: snapnum, positions and velocities of each halo, its mass (M_{200c}200) and spin.

A10 Munich - SAGE (Croton)

The new Semi-Analytic Galaxy Evolution (SAGE) model is an updated version of that first presented in Croton et al. (2006). We only

highlight the significant changes here and point to the 2006 paper and Croton et al. (in prep.) for a full description of the rest of the model.

SAGE is publicly available through the Theoretical Astrophysical Observatory[9] (TAO; Bernyk et al. 2014), an online virtual laboratory that includes tools to add hundreds of magnitude filters to the galaxy output (with or without dust), construct custom light-cones, build images, and then download the mock data to your local machine, all without any requisite programming knowledge.

Cooling Cooling is handled as in Croton et al. (2006). An isothermal sphere is assumed and a cooling rate estimated from a simple continuity argument.

Star formation The SAGE model calculates the mass of cold gas in the disk that is above a critical surface density for star formation. New stars then form from this gas using a Kennicutt-type prescription.

Initial mass function SAGE assumes a Chabrier (2003) IMF.

Metal treatment SAGE follows the simplistic metal treatment introduced in De Lucia et al. (2004a). A yield of metals is produced from each star formation event and is recycled instantly back to the cold gas from very short-lived stars.

Supernova feedback and winds Feedback from supernova in SAGE is a two step process. First, an assumed mass loading factor pushes cold gas out of the disk into the hot halo. Second, if enough energy from supernova has been added to the hot halo carried by this gas, some of the hot gas becomes unbound and is removed to an ejected reservoir.

Gas ejection & reincorporation Gas can be ejected from the halo from supernova or quasar winds. Ejected gas can be reincorporated back into the hot halo at a rate in proportion to the dynamical time of the dark matter halo.

Disk instability SAGE uses the Mo et al. (1998) approximation to determining when a disk becomes unstable. When so, enough existing stars are transferred to the bulge to make the disk stable, along with any new stars as a result of a starburst.

Starburst The SAGE model applies the collisional starburst model introduced in Somerville et al. (2001) to determine the mass of cold gas that becomes new stars during a merger.

AGN feedback SAGE uses the radio-mode AGN heating model introduced in Croton et al. (2006), and a new quasar-mode wind model introduced in Croton et al. (in prep.).

Merger treatment Mergers are treated using the method described in Croton et al. (in prep.). Satellites are either merged with the central galaxy or added to the halo's intra-cluster stars, depending on the subhalo survival time relative to an average expected based on its infall properties.

Substructures Substructures are explicitly followed from the N-body simulation.

Orphans No orphans are used in SAGE. A decision as to the fate of a satellite galaxy has already been made and executed before its subhalo is lost below the resolution limit of the simulation.

Calibration method SAGE is calibrated by hand using the $z = 0$ stellar mass function, cold gas fraction, stellar metallicity–stellar mass relation, baryonic Tully-Fisher relation, and black hole–bulge mass relation.

Model origin SAGE is an evolution of the LGALAXIES semi-analytic code which is based solely on N-body simulations.

Modifications to the supplied data No modification were made to the supplied data.

Halo finder properties used The primary mass used was M_{200c}. Additional halo finder properties used to build galaxies are the peak value of the circular rotation curve, the position, and the spin parameter.

A11 HOD – MICE (Castander & Carretero)

The MICE project[10] is producing large simulations to help the design and interpretation of large scale cosmological observational projects. In this paper, we use the galaxy mock generation code that has been developed within MICE. The galaxy mock code populates dark matter haloes with a hybrid Halo Occupation Distribution (HOD; Jing et al. e.g., 1998; Scoccimarro et al. e.g., 2001; Berlind & Weinberg e.g., 2002) and SubHalo Abundance Matching (SHAM; Vale & Ostriker e.g., 2004; Tasitsiomi et al. e.g., 2004; Conroy et al. e.g., 2006) technique (Carretero et al. 2015; Castander et al. 2014; Crocce et al. 2013). Following the HOD philosophy, we assume that haloes are populated by central and satellite galaxies. We assign luminosities to central galaxies based on abundance matching taking into account the scatter between halo mass and luminosity. The HOD gives us the number of satellites in each halo. The satellite luminosities are drawn from the satellite luminosity function. We distribute satellites inside the haloes following a triaxial 'modified' NFW, tweaked to match the observed clustering. The HOD parameters are also varied until we find an acceptable fit to the galaxy clustering as a function of luminosity. We assign velocities to the galaxies assuming a Gaussian velocity dispersion distribution given by the halo mass (Bryan & Norman 1998). Lastly, we assign colours and SEDs with recipes that fit the clustering as a function of colour. We calibrate our method with local constraints given by the Sloan Digital Sky Survey (SDSS; York & et al. 2000) using the MICE Grand Challenge simulation (Fosalba et al. 2013; Crocce et al. 2013; Fosalba et al. 2013; Hoffmann et al. 2015) as starting halo catalogue. In particular we reproduce the galaxy luminosity function (Blanton & et al. 2003; Blanton et al. 2005b), the colour-magnitude diagram (Blanton et al. 2005) and the SDSS clustering properties as a function of luminosity and color (Zehavi et al. 2011). We extend our recipes to higher redshift applying evolutionary corrections to the galaxy colours and then resampling from the cosmos catalogue (Ilbert & et al. 2009) galaxies with compatible luminosities and colours at the given redshift.

Cooling —

[9] https://tao.asvo.org.au

[10] http://www.ice.cat/mice

Star formation We obtained the star formation rate from the dust-corrected UV flux of the galaxy SED.

Initial mass function We assume a 'diet' Salpeter IMF (Bell & de Jong 2001).

Metal treatment We compute the metallicity from the absolute magnitude using empirically determined relations.

Supernova feedback and winds —

Gas ejection & reincorporation —

Disk instability —

Starburst —

AGN feedback —

Merger treatment —

Substructures We use a hybrid method to treat substructures. We can use the substructures provided by N-body, but if they are not available we can generate them analytically.

Orphans We compute the expected number of satellites for each halo following an HOD prescription. If the halo contains fewer subhaloes, we generate as many new satellites as the HOD predicts. We call these new satellites orphans in this context. We place them in the halo following a NFW profile with a concentration index expected for its halo mass.

Calibration method The method has been calibrated to reproduce the galaxy luminosity function, the colour magnitude-diagram and the galaxy clustering as a function of luminosity and colour. The calibration is performed at low redshift and extrapolated at higher redshifts. The calibration has been done minimizing a χ^2, where we have altered the input parameters manually. Note that our method has only been calibrated out to redshift z=1.5 and although we have computed quantities at higher redshifts in this paper, they are just an extrapolation of our recipies that we have not calibrated. So, take that in mind when trying to interpret the MICE results beyond that redshift.

Model origin The model stems from N-body simulations, namely the MICE Grand Challenge N-body simulation.

Modifications to the supplied data The supplied data has not been modified

Halo finder properties used The base for our method are the halo masses and we adopted $M_{\rm fof}$ as the choice for the data presented here. We further use the following properties from the input catalogue: haloid, hosthaloid, number of substructures, number of particles, position, velocity, radius, peak value and position of the circular rotation curve, velocity dispersion, and concentration.

A12 HOD – SKIBBA (Skibba)

The model used for this work is based on the halo model of galaxy clustering developed in Skibba et al. (2006) and Skibba & Sheth (2009). 'Central' and 'satellite' galaxy luminosities are modelled such that the luminosity function and luminosity dependence of clustering are the same as that observed. All galaxy properties and their occupation distributions are determined by halo mass, concentration, and halo-centric position; therefore, all environmental correlations are entirely a consequence of the fact that massive haloes tend to populate dense regions (i.e., no 'assembly bias' is assumed). Satellites are assigned to subhaloes in the simulation, assuming an abundance matching-like procedure that includes scatter between stellar mass, subhalo mass, and $V_{\rm max}$. To include colours, we develop a prescription for how the colour-luminosity distribution of central and satellite galaxies depends on halo mass, and this model is consistent with the observed colour mark correlation function. I assume that the fraction of satellite galaxies which populate the red sequence increases with luminosity, and this fraction is in agreement with galaxy group catalogues (Skibba & Sheth 2009) and with the gradual quenching of satellites' star formation Font et al. (2008). Stellar masses are based on luminosities and colors; since these are consistent with observations, it is not surprising that the stellar mass function and clustering are consistent with observations as well. It is important to note that the model's observational constraints are robust only at $M_* > 10^9 h^{-1}{\rm M}_\odot$ and $M_{\rm halo} > 10^{11} h^{-1}{\rm M}_\odot$; therefore, I have applied a mass threshold, below which this model should not be extrapolated or compared to other models (or to observations).

We have made many updates and improvements to the model, which will be described in Skibba (in prep.). We are including colour and stellar mass gradients within haloes (Hansen et al. 2009; van den Bosch et al. 2008) and a dependence of the colour distribution on halo mass at fixed luminosity (More et al. 2011; Hearin & Watson 2013). In addition, the model includes a treatment of dynamically unrelaxed systems, including some non-central brightest halo galaxies, the fraction of which is constrained by SDSS and mock group catalogues (Skibba et al. 2011; Skibba & Macciò 2011).

The model provided here is a sort of HOD-SHAM hybrid, in which I populated subhaloes when possible and when an insufficient number of resolved subhaloes were found, I distributed the satellites with my model's standard prescription. I generously populated low-mass subhaloes in this model, and as a result the orphan fraction is relatively low.

Cooling —

Star formation The model currently only includes optical colours; a subsequent version will include a model of star formation rates. The model's stellar masses apply a calibration from Zibetti et al. (2009).

Initial mass function A Chabrier (2003) IMF is used throughout.

Metal treatment Gas-phase and stellar metallicities are based on scaling relations of Tremonti et al. (2004) and Gallazzi et al. (2005).

Supernova feedback and winds —

Gas ejection & reincorporation —

Disk instability Disk instabilities are not included in the model, but spiral and elliptical morphologies are included based on clustering and other constraints from Skibba & Sheth (2009).

Starburst —

AGN feedback AGN feedback is not modelled here, but a simple black hole mass scaling relation basted on Tundo et al. (2007) is applied.

Merger treatment —

Substructures Substructure properties are taken from the simulation at a given snapshot, but subsequent subhalo evolution is not modelled.

Orphans When a sufficient number of substructures are not resolved to match them to satellites, haloes are populated with the remaining satellites ('orphans') in order to reproduce the model's occupation distributions. Orphans are spatially distributed with a Navarro et al. (1997, NFW) profile with the Macciò et al. (2008) mass-concentration profile is assumed, while accounting for the fact that galaxies and subhaloes are typically less concentrated than dark matter Munari et al. (2013).

Calibration method The model has been designed to reproduce real- and redshift-space luminosity and colour-dependent galaxy clustering (Zehavi et al. 2011) and mark clustering statistics (Skibba et al. 2006). The model is also constrained by the SDSS luminosity function (Blanton & et al. 2003; Yang et al. 2009) and colour-luminosity distribution (Skibba & Sheth 2009). The model is consistent with the Moustakas et al. (2013) stellar mass function, which is not used as a constraint. The model is consistent with the Moustakas et al. (2013) stellar mass function, which is not used as a constraint though.

Model origin The model originates from an analytic halo-model formalism (Cooray & Sheth 2002).

Modifications to the supplied data No modification were made to the supplied data.

Halo finder properties used The model uses the 3-D positions, 3-D velocities, halo mass and radius (200c and bound), V_{max}, velocity dispersion (200c), and the substructure abundances and properties.

Because the observational constraints are less robust at low masses and luminosities, we have applied a halo mass threshold near $10^{11}h^{-1}\mathrm{M}_{\odot}$. The SKIBBA model is complete only above this mass.

APPENDIX B: HALO-MASS DEFINITION

While we have already discussed the influence of the applied mass definition on the model-to-model variation seen in Section 5 we like to extend this here a bit more by directly comparing two mass definitions on a model-by-model basis. Namely, for those models that provided both an M_{200c} galaxy catalogue and a catalogue based upon their own mass definition (different from M_{200c}, of course) we show in Fig. B1 the stellar mass functions: solid lines are for the model mass definition whereas dotted lines are for M_{200c}. Some models appear to be sensitive to the choice of the definition for halo mass, but the overall level of scatter across various models seems to stay similar. We append some more plots that focus on the redshift evolution as this is where the mass definition leaves its largest imprint. The plots are accompanied by Table B1 where we list the number of galaxies in various populations. This table should be compared against Table 3.

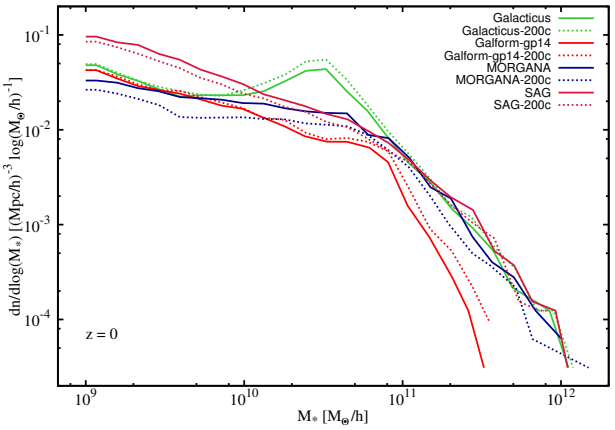

Figure B1. Stellar mass function at redshift $z = 0$ for models that also provided data for M_{200c} as the mass definition. To be compared against Fig. 2.

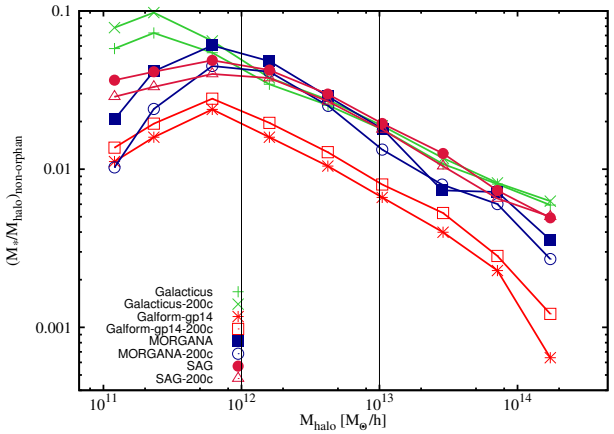

Figure B2. Stellar-to-halo mass ratio for all (non-orphan) galaxies at redshift $z = 0$. To be compared against Fig. 10.

APPENDIX C: INITIAL STELLAR MASS FUNCTION

As the change in stellar mass will also influence the number of galaxies above our usual threshold $10^{9}h^{-1}\mathrm{M}_{\odot}$ we also list the (change in) numbers in Table C1, only showing the affected models. This table should be compared against Table 3 again.

APPENDIX D: UN-NORMALIZED REDSHIFT EVOLUTION

In Section 6 we discussed the redshift evolution of both the number (density) of galaxies and the star formation rate (density), normalizing the respective curves to their redshift $z = 0$ values. The normalizations have been provided in Table 2 & Table C1 and hence we separated 'trends' (as shown in the figures) from 'absolute'

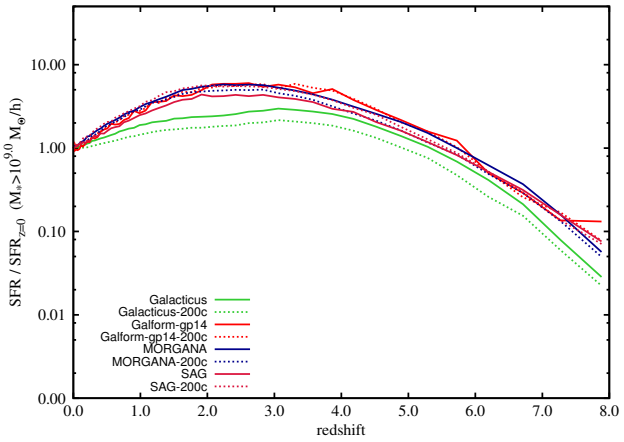

Figure B3. Star formation rate density as a function of redshift for models that also provided data for M_{200c} as the mass definition. To be compared against Fig. 7.

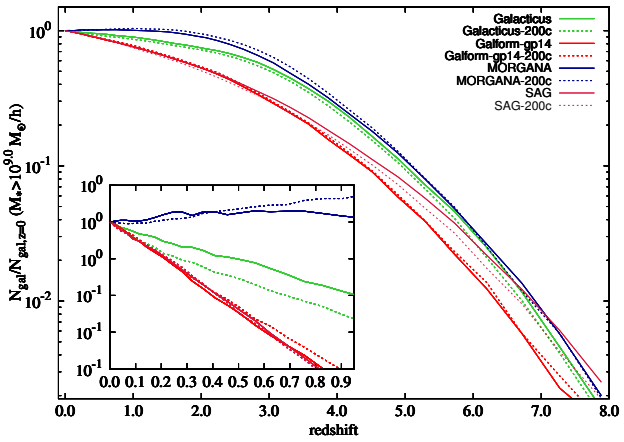

Figure B4. The number density of all galaxies with stellar mass $M_* > 10^9 h^{-1}\mathrm{M}_\odot$ as a function of redshift for models that also provided data for M_{200c} as the mass definition. To be compared against Fig. 11.

Table B1. Number of galaxies at redshift $z = 0$ with a stellar mass in excess of $M_* > 10^9 h^{-1}\mathrm{M}_\odot$ for models when applying M_{200c} as the mass definition ($-200c$ extension) and when using their favourite mass definition. Note again that for MORGANA all satellites have been tagged as 'orphan'.

code name	$N_{\rm gal}^{z=0}$	$N_{\rm central}$	$N_{\rm non-orphan}^{z=0}$	$N_{\rm orphan}^{z=0}$
GALACTICUS	14255	7825	10019	4236
GALACTICUS$-200c$	16123	9026	11393	4730
GALFORM-GP14	8824	5097	6098	2726
GALFORM-GP14$-200c$	9320	5595	6666	2654
MORGANA	10008	6186	6186	*3822*
MORGANA$-200c$	7316	4925	4925	*7316*
SAG	19516	13571	16256	3260
SAG$-200c$	16505	11332	13773	2732

Table C1. Number of galaxies at redshift $z = 0$ with a stellar mass in excess of $M_* > 10^9 h^{-1}\mathrm{M}_\odot$ for those models that have been affected by the transformation to a Chabrier IMF. To be compared against Table 3.

code name	$N_{\rm gal}$	$N_{\rm central}$	$N_{\rm non-orphan}$	$N_{\rm orphan}$
GALICS-2.0	tuned parameters to observations w/ Chabrier IMF			
SAG	14025	9565	11758	2267
Durham flavours:				
GALFORM-GP14	9842	5680	6770	3072
GALFORM-KB06	10467	6060	7225	3242
GALFORM-KF08	13340	7054	8371	4969
HOD models:				
MICE	9510	5638	8067	1443

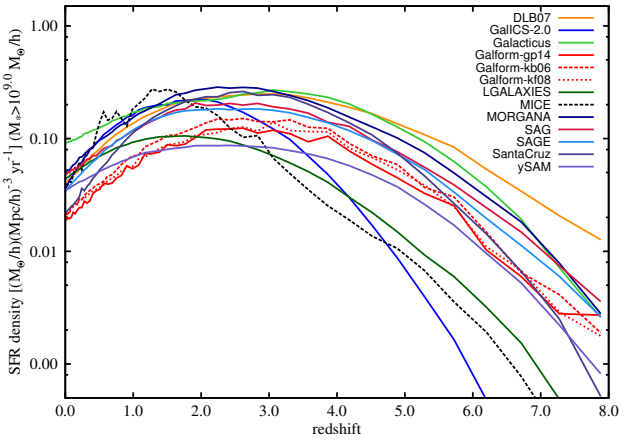

Figure D1. Star formation rate density as a function of redshift.

differences (as listed in the tables). Here we now provide the unnormalized plots directly showing the different evolutions for both these quantities.

This paper has been typeset from a TEX/ LATEX file prepared by the author.

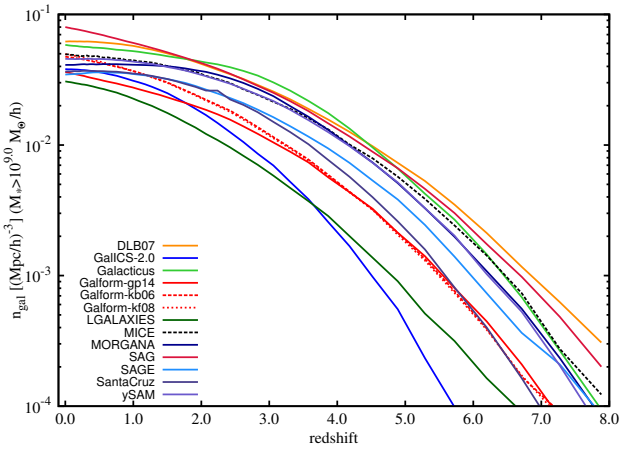

Figure D2. The number of all galaxies with stellar mass $M_* > 10^9 h^{-1}\mathrm{M}_\odot$ as a function of redshift.